TÉCNICO LISBOA

Characterization and Gas Permeation Properties of Blood Compatible Membranes for Blood Oxygenators

Ana Rita Gonçalves Varandas Martins

Thesis to obtain the Master of Science Degree in

Chemical Engineering

Supervisors: Dr. Mónica Cristina Faria Besteiro
Dr. Pedro Jorge Rodrigues Morgado

Examination Committee

Chairperson: Prof. Dr. Carla Isabel Costa Pinheiro
Supervisor: Dr. Pedro Jorge Rodrigues Morgado
Member of the Committee: Prof. Dr. Isabel Maria Delgado Jana Marrucho Ferreira

October 2019

Acknowledgments

First and foremost, I would like to thank my supervisors Dr. Pedro Morgado and Dr. Mónica Faria not only for all their time in explaining and clarifying doubts both in the experimental execution and theoretical matters, but also for the guidance and advice given.

Next, but not less important, I would like to convey my appreciation to Professor Eduardo Filipe for proposing the theme and giving me the opportunity to carry out the present work.

I would also like to express my appreciation to Tiago Eusébio for his help in understanding the experimental set-up and solving problems related to it, as well as for his contribution in the initial phase of membrane preparation in the laboratory.

I am grateful for all the support and motivation given by my friends and colleagues. A special thanks to Sara Pinhão for never letting me quit and Rui Almeida for being present in the majority of the time during the execution of experiments, as well as the rest of the degree.

To all members of my previous laboratory and project groups: Ana Carolina Alves, Beatriz Mendes and João Gaspar, I really appreciate you and I am thankful for all the fellowship and hours spent studying, without whom it would not have been possible to finish the degree in such a positive way. It is only fair to acknowledge also the companionship of my truly important friends Beatriz Soares and Joana Richheimer, who despite being far away, were always available to talk.

Finally, to my mom and dad, thank you for the opportunity to pursue a higher education and for providing me with all the conditions and resources to do so. In addition, I am grateful for all the unconditional support, motivation and positivity.

Abstract

Nonporous and Integral Asymmetric bi soft segment Poly(ester urethane urea) membranes were prepared including Polycaprolactone (PCL) as a second soft segment, using the solvent evaporation method and a modified version of phase inversion technique, respectively. The synthesis was performed by reacting a combination of Polyurethane (PUR) and Polycaprolactone-diol prepolymers in a solvent mixture comprising Dimethylformamide (DMF) and Diethyl ether (DEE).

Several casting solutions were made with a total polymer/solvent weight ratio of 65/35, a DMF/DEE ratio of 3/1 wt.% and varying the PUR/PCL weight ratio (100/0, 95/5, 90/10 and 85/15). For asymmetric membranes, solvent evaporation times of 1, 5 and 10 minutes were studied. Samples were analysed by Scanning Electron Microscopy (SEM).

Using an existing gas permeation setup it was possible to determine the permeances for the two groups of membranes. Plus, applying the time lag method to the same results allowed the determination of the diffusion and solubility coefficients. All results showed the same order of magnitude.

No immediate correlation was identified between the properties studied due to its nonlinear behavior, however, from the overall comparison, the best compositions and, consequently, preparation methods were revealed to be 5% PCL with 5 minutes of solvent evaporation time and 15% PCL with 1 minute. Estimates made on the thickness of the dense layer revealed that the synthesis of asymmetrical membranes allowed a reduction of this variable, in contrast to fully dense membranes, representing an improvement in gas permeation.

Keywords: Membrane blood oxygenators, Bi soft segment Poly(ester urethane urea) membranes, Integral asymmetric membranes, Gas permeation, Time lag method.

Resumo

Sintetizaram-se membranas não porosas e integralmente assimétricas de Poli(éster uretano ureia) com dois segmentos flexíveis, incluindo na sua estrutura Policaprolactona (PCL) como segundo segmento. Estas foram preparadas fazendo reagir uma mistura de dois pré-polímeros: Poliuretano (PUR) e Policaprolactona-diol, com uma mistura de solventes composta por Dimetilformamida (DMF) e Éter Dietílico (DEE), utilizando o método de evaporação do solvente e uma versão modificada da técnica de inversão de fase, respectivamente.

Diversas soluções de casting foram preparadas com um rácio mássico polímero/solvente de 65/35 e DMF/DEE de 3/1, variando a proporção PUR/PCL (100/0, 95/5, 90/10 e 85/15). Para as membranas assimétricas, foram ainda estudados tempos de evaporação do solvente iguais a 1, 5 e 10 minutos. Todas as amostras foram analisadas por Microscopia Electrónica de Varrimento (MEV).

Através de um sistema de permeação gasosa já existente foram determinadas as permeâncias para os dois grupos de membranas. Para além disso, a aplicação do método time lag aos mesmos resultados permitiu o cálculo dos coeficientes de difusão e solubilidade. Todos os resultados apresentaram a mesma ordem de grandeza.

Devido ao comportamento não linear entre as propriedades estudadas, não foi possível identificar uma correlação direta. No entanto, as composições que apresentaram os melhores desempenhos e, consequentemente, métodos de preparação adequados foram as membranas com 5% PCL e 5 minutos de evaporação do solvente, assim como, as membranas de 15% PCL com 1 minuto de evaporação. Estimativas realizadas à espessura da camada densa revelaram que a síntese de membranas assimétricas permitiu uma redução desta variável em contraste com as membranas totalmente densas, corroborando a melhoria verificada na permeação gasosa.

Palavras-Chave: Oxigenadores de sangue, Membranas de Poli(éster uretano ureia) com dois segmentos fléxiveis, Membranas assimétricas, Permeação gasosa, Método time lag.

Contents

List of Tables

List of Figures

Acronyms

DEE Diethyl Ether. 10, 18, 19, 23, 45, 46

DMF Dimethylformamide. 10, 18, 19, 23, 45, 46

DMTA Dynamic Mechanical Thermal Analysis. 8

ECMO Extracorporeal Membrane Oxygenation. 1–3, 47

HS Hard Segments. 5, 7–9, 17

PAN Polyacrylonitrile. 4

PBDO Poly(butadienediol). 7

PCL Poly(caprolactone). 7–9, 11, 17–19, 23, 27, 28, 31–36, 38, 40–46

PDMS Poly(dimethylsiloxane). 7

PE Polyethylene. 4

PEI Polyether imide. 4

PET Polyethylene terephthalate. 4

PEUU Poly(ester urethane urea). 7–9, 11, 17–19, 28, 30, 36, 41, 43, 45, 46

PfT Feed Pressure Sensor. 20, 21

PMMA Poly(methylmethacrylate). 4

PMP Polymethylpentene. 28

PP Polypropylene. 28

PPO Poly(propylene oxide). 7, 9, 11, 17

PpT Permeate Pressure Transmitter. 20, 21

PRV pressure reducing valve. 21

PTFE Polytetra-fluoroethylene. 4

PU Polyurethane. 4, 5, 7–11, 45

PUR Polyurethane prepolymer. 17, 28

SEM Scanning Electron Microscopy. 11, 20, 23–25, 32, 45, 46

SS Soft Segments. 5, 7–9, 11, 17, 18

STP Standard conditions for temperature and pressure. 26

TMP Transmembrane Pressure. 26, 27, 36, 38

UTS Ultimate Tensile Strength. 8

List of Symbols

A – Effective membrane area

α – Selectivity

D – Diffusion Coefficient

δ – Total membrane thickness

J – Flux

P – Permeability

p – Pressure

$Perm$ – Permeance

p_f – Feed pressure

p_p – Permeate pressure

p_{pi} – Inicial permeate pressure

p_{STP} – Pressure in STP conditions

R – Ideal gas constant

S – Solubility

T – Temperature

V – Volume

V_s – Volume of the receiving chamber

V_{STP} – Volume in STP conditions

Chapter 1

Introduction

1.1 Extracorporeal Membrane Oxygenation (ECMO)

ECMO, also known as Extracorporeal Membrane Oxygenation, is a procedure used to oxygenate blood, as well as removing carbon dioxide from it, without the need for native lungs. On that note, the equipment takes over the work of the lungs, heart or both when these organs are too damaged to perform their function properly, allowing the healing process to occur, or during surgery. It is known that, in 2005, approximately 1.2 million operations were carried out using ECMO, corresponding to a consumption of 3 million km of oxygenation membranes [1].

This extracorporeal life support consists in an external artificial circulation that carries venous blood, lacking in O_2 content but rich in CO_2, from the patient to a gas exchange device where blood then becomes enriched with the first mentioned above and has carbon dioxide removed. The exchange is achieved by feeding the said gases and a sweep gas to a compartment divided by a membrane. This device is called an oxygenator and the blood is then warmed and returned to the body [2].

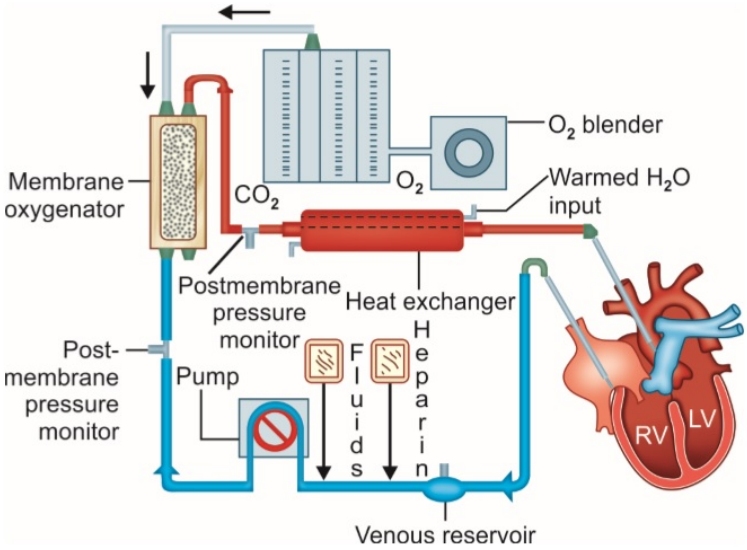

Figure 1.1: Simplified ECMO scheme [2].

Therefore, ECMO is a temporary support of the heart and lung function by a partial cardiopulmonary bypass (up to 75% of cardiac output), normalizing oxygen delivery, and it has its use in cardiopulmonary surgery, heart valve replacement, traumatic injuries, infections or inflammations of the lungs. Also, it can

be helpful in lung transplants, maintaining the gas levels stable during the intervention and even to allow the patients to remain awake and ambulatory while awaiting a donor organ [1, 2].

In the time being, there are two types of ECMO. One is called Venovenous (VV) and is usually performed for isolated respiratory failure, providing lung support only. The other one is Veno-arterial (VA) and it is prepared to deal with both cardiac and respiratory failure combined, providing heart and lung support. The main difference lies in the place where the blood re-enters the patient's circulation, i.e, blood is removed from venous side and then pumped back into it on the first one, contrasting with the second option, where blood is pumped to arterial side instead.

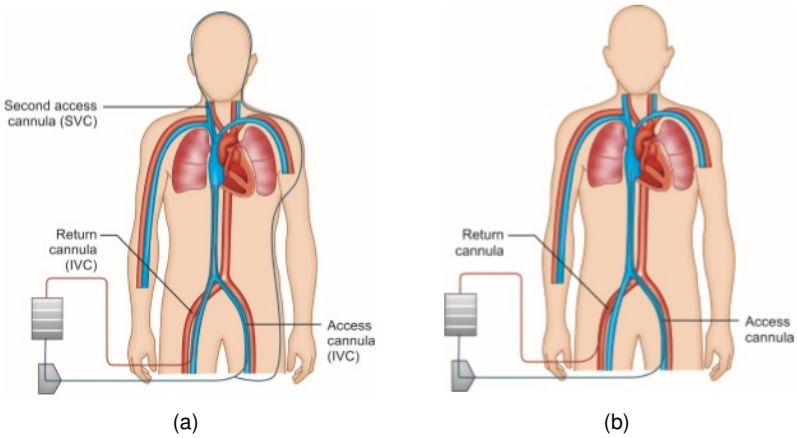

Figure 1.2: Types of ECMO circuits: (a) Venovenous; (b) Veno-arterial [2].

Since in this type of treatment remains the need to use a medicine that thins the blood to avoid the formation of clots (anticoagulation), usually Heparin, the biggest risk of ECMO is bleeding. Plus, oxygenator and circuit priming volumes in excess of 100 mL often require blood transfusions to initiate the exchange, especially for pediatric and neonatal patients [2].

1.2 Natural Lung vs. Oxygenator

In the natural human lung, both blood and gas are separated by the alveolar capillary wall having no direct contact. The gas transfer then obeys the laws of diffusion, exchanging the O_2 and CO_2 between the alveolar air and the pulmonary capillary blood [3]. This means that deoxygenated blood enters the pulmonary circulation and passes through the lungs where it gets oxygenated. Lastly, oxygenated blood enters the systemic circulation through the pulmonary vein [2].

The exchange itself is very efficient due to the large surface area provided by the capillary network, capable of oxygenating larger quantities of air than required. The total exchange membrane area is around 80 m^2. Thus, people with impaired lung capacity can generally live a normal life [4].

The ideal oxygenator must be capable of performing an efficient gas exchange and, at the same time, should be gentle to the blood. More specifically, it should be able to oxygenate up to 5 L/min of venous blood to 95-100% haemoglobin saturation for periods between some minutes (20 min) till several hours. In addition, it has to assure a certain removal of CO_2 in order to avoid respiratory acidosis or alkalosis, to undertake a reasonable blood priming volume (1-4L) and to operate in a simple and safe manner [4].

In particular, the oxygenator must deliver about 250 cm^3 (STP)/min O_2 and remove about 200 cm^3 (STP)/min CO_2. The solubility of these gases into the blood is limited, therefore a high blood flow through the device is required (2–4 L/min). Note that the driving force for O_2 is 15 times that for CO_2. In the lung,

the ratio is about 13 times, but this organ is over 20 times more permeable to CO_2 than to O_2. Therefore, the key consideration in the design of a membrane oxygenator is the CO_2 transport [4].

In order to maintain oxygen transfer effective, from the surface of the gas exchange membrane to the plasma and then to red cells, the distance of gas transfer should always be kept to a minimum [3].

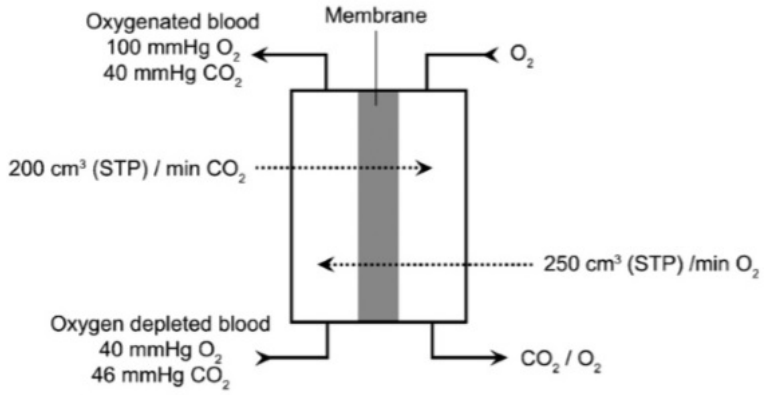

Figure 1.3: Principle of the membrane blood oxygenation [4].

The first successful long-duration use of ECMO to support a human patient was reported in 1972, using a Bramson oxygenator. The latter consists in a 6 m^2 parallel plate system comprised of 15 individually transfused blood channels to enable the recovery from “shock lung” or acute respiratory distress syndrome, over a period of 75 h [2].

1.3 Evolution of Oxygenators

In the history of oxygenators, three different types are known: film, bubble and membrane. The first one consists in producing a thin blood film where the gas exchange takes place on the surface of the exposed blood film. Secondly, bubble type oxygenators work by introducing gas directly into the blood in the form of bubbles. In this type of equipment, gas exchange is enhanced due to the large surface area of the bubbles which makes it one of the most effective. On the other hand, introducing air bubbles directly into the blood cause mechanical stress on the system, leading to higher levels of trauma.

Lastly, there are several types of membrane oxygenators, for example: plate-type membrane, disposable coiled membrane and hollow-fibre. As said before, in these cases, the blood is exposed to oxygen through a gas permeable membrane and because direct contact is not promoted, the trauma is minimal, being considered the most atraumatic option. However, the surface area applied must be larger to compensate the resistance introduced by the membrane to the permeating gases.

Comparing all the options, oxygenators have an equal capability for oxygenating venous blood, but membrane ones require a smaller volume for priming to achieve a sufficient gas transfer rate, also contributing for less blood trauma such as hemolysis, because it uses a similar mechanism to the natural lung [1, 3]. Nowadays, membrane oxygenators have around 0.5 to 2.5 m^2 of active area, which means that this number corresponds only to 10% of a natural lung of an adult and even young children, so it is necessary to control different parameters like partial pressure difference or contact time [1].

The first and most used oxygenator in the clinical field, from the 1950s up to the 1980s, was the bubble oxygenator. However, later in the 1980s, the first capillary type oxygenator adopted the system of intracapillary (luminal flow) blood perfusion. Unfortunately, the latter induced high pressure resistance in the module and caused hemolysis, required larger membrane quantities and priming volumes and had poor biocompatibility. For that reason, currently, capillary oxygenators commonly adopt the system

of extracapillary (extraluminal) blood perfusion, capable of providing better mixing of the blood and thus improve the O_2 transfer rates [1].

1.4 Factors affecting Gas Transfer in Blood Oxygenators

One of the main problems the science community faces when developing membranes for oxygenators, besides compatibility and degradability issues, is the efficiency of gaseous transport. In artificial lungs, factors affecting oxygen transport are related with the concentration of the said gas in sweep gas, the blood partial pressure in this fluid, membrane diffusion characteristics and surface area and, finally, blood flow rate itself.

On the other hand, besides the physical properties of the membranes mentioned above, transport of CO_2 includes cardiac output and pulmonary perfusion. Moreover, the transport depends on sweep gas flow rate, to the extent that increasing the total flow rate by increasing the O_2 flow will result in decrease in concentration CO_2 gas in sweep gas across the membrane and thus decreasing the CO_2 content in the blood. However, CO_2 transport is independent of blood flow rate, membrane thickness and blood path size [2].

1.4.1 Deposition

One of the problems that directly affects the efficiency of an oxygenator is the deposition of plasma proteins during treatment. These proteins adsorb at the membrane's surface continuously, causing accumulation and intensifying the layer length, growing also through the pores. This leads to an increase of surface energy and, consequently, the pores become wet causing plasma breakthrough from the blood side to the gas side [1].

In blood-contact membranes, proteins adsorption-caused fouling results in a progressive decline in flux and affects the membrane selectivity. Such adsorption can also initiate processes of activation of different defense systems in blood, for example coagulation, or promote adhesion and activation of blood cells. Besides protein fouling, there is concentration polarization which is the solute accumulation near the membrane surface resulting in a concentration gradient [4, 5]. However, unlike concentration polarization, protein adsorption/depositon on the surface or in the pores is irreversible in nature and it can affect the biocompatibility of the membrane. Factors that can influence this effect are related to its surface chemistry, adsorbed protein size, charge, shape or pH value.

Therefore, asymmetric membranes are in advantage behaving as surface filters. By this, it means they can retain all rejected materials on the surface, where most of them could be removed by shear forces applied by the feed, opposing to symmetric ones that act like depth filters and retain most particles within their internal structure.

Diffusion can, in fact, initiate swelling and leaching phenomena. Swelling involves transport of ions or fluid leading to static fatigue or crazing of the material, once its elastic limit is reduced. On the other hand, leaching occurs if the biomaterial dissolves into the surrounding fluid, in this case blood, causing local biological reactions, fracture strength and elastic modulus decay of the material [4].

1.4.2 Degradation

In the polymer family, there are some choices considered to have minimal degradation that include: Polyethylene terephthalate (PET), Nylon 6.6, Polyurethane (PU), Polytetra-fluoroethylene (PTFE), Polyethylene (PE), Polysiloxanes and Poly(methylmethacrylate) (PMMA), modified Polyacrylonitrile (PAN) and Polyether imide (PEI) [4].

Now focusing on the class of the polyurethanes, these polymers are segmented elastomers with two distinct phases: glassy or semicrystalline urethane hard phase dispersed in a viscous or rubbery macroglycol matrix soft phase, which gives exceptional physical and mechanical properties to these polymers. This class also shows good biocompatibility [6, 7].

There are several chemical compositions of commercially available and experimental PU's due to the diverse types of chemical structures that can be present in both Soft Segments (SS), which has a polyether or polyester structure, as well as in the Hard Segments (HS), composed of a chain extender and a diisocyanate, being the polyether ones the most commonly used in biomedical applications [7].

As a result of the composition described, PU's can suffer diverse types of degradation [7] to name a few:

- Hydrolytic degradation, when the urethane and urea structures are inherently hydrolysable. It is important to mention that a polyether-based PU formulation shows no evidence of degradation in samples aged at a temperature of 37^{o}C;
- Oxidative degradation, when the polyether segment is thought to be the most susceptible to oxidative breakdown, unlike in the previous kind of degradation, where it is highly resistant to hydrolysis. However, although under normal atmospheric conditions polyurethanes are relatively stable, if metabolic products are present, they might have enough oxidative strength to enhance the degradation reactions;
- Enzymatic degradation;
- Calcification. This type of degradation is caused by complexation of metal ions and it can affect the mechanical properties of the polymer or decrease its chemical stability. The chemical groups capable of chelating metal ions are present in both soft and hard segments. As mentioned before, biocompatibility is related to the surface chemistry. Consequently, chemical composition of the PU surface is crucial and determines the interactions between the polymer and the host body.

In order to prevent degradation, there are several methods to modify the surface properties, for example: introduce negatively charged surface groups, biomimetic modifications, introduce steric hindrance or increase hydrophilicity [4]. In fact, surface electrical properties play a role in polymer interactions with blood and hydrophilicity may affect hemocompatibility through alteration of the structure of water at the interface [6, 8].

Chapter 2

State of the Art

2.1 Modified Polyurethanes - Bi soft segment Membranes

Bi soft segment membranes are characterized by the presence of two different types of Soft Segments (SS), as the name implies. Studies carried out by Faria et. al [9] included the preparation of different kinds of Polyurethane membranes that fulfill a twofold goal: exhibit enhanced hemocompatibility and have suitable gas permeation rates. For this membranes the preparation included Poly(butadienediol) (PBDO) or Poly(dimethylsiloxane) (PDMS).

For the PU/PBDO membranes phase segregation studies showed the existence of hydrogen bonded HS's with formation of urethane/urea aggregates. When the PBDO content is increased, a higher percentage of mixing between the two SS is observed as well as a decrease of the urethane/urea aggregation [10]. Tests revealed that the ratio of PU to PBDO affects the CO_2 permeability of the membranes. Membranes containing 20 wt.% and 67 wt.% of PBDO had a CO_2 permeability of 150 Barrer and 90 Barrer, respectively. Furthermore, in this case, larger quantities of the second SS led to higher degrees of mixing between microphases which led to lower CO_2 permeabilities [9]. Lastly, the introduction of PBDO turned the hemolytic into non-hemolytic membranes and, for blood contact times of 10 and 15 minutes, it decreased its thrombogenicity [11].

Regarding the PU/PDMS membranes containing 25 wt.% to 75 wt.% of PDMS, results showed evidence of phase separation between the two SS. For membranes with lower contents of PDMS, the structures analysis demonstrated that the HS formed aggregates and that these decreased with the increase of PDMS content. The 25 wt.% and 75 wt.% of PDMS ones had CO_2 permeability of 200 Barrer and 800 Barrer, respectively, and O_2 permeability of 30 Barrer and 120 Barrer, respectively. Finally, it was perceptible that the CO_2 and O_2 permeability of the membranes rose with the increase of PDMS while the permeability ratios $P(CO_2)/P(N_2)$ and $P(O_2)/P(N_2)$ did not varied significantly, being the high permeability of the 75 wt.% membrane attributed to the higher content of siloxane groups, lower degree of cross-linking and lower aggregation of urethane/urea groups [9, 12].

2.2 Bi soft segment Polyurethane Membranes - PU/PCL

More specifically, segmented polyurethane urea membranes containing Poly(propylene oxide) (PPO) and Poly(caprolactone) (PCL) have been usually prepared by extending a Poly(propylene oxide) based tri-isocyanated prepolymer with Poly(caprolactone) diol.

In the synthesis, PCL was selected as the second Soft Segment because of its established use in vascular tissue engineering [13]. However, due to its intrinsic biodegradability, the use of Poly(ester

urethane urea) (PEUU) membranes is limited to medical device applications requiring short-term contact with blood.

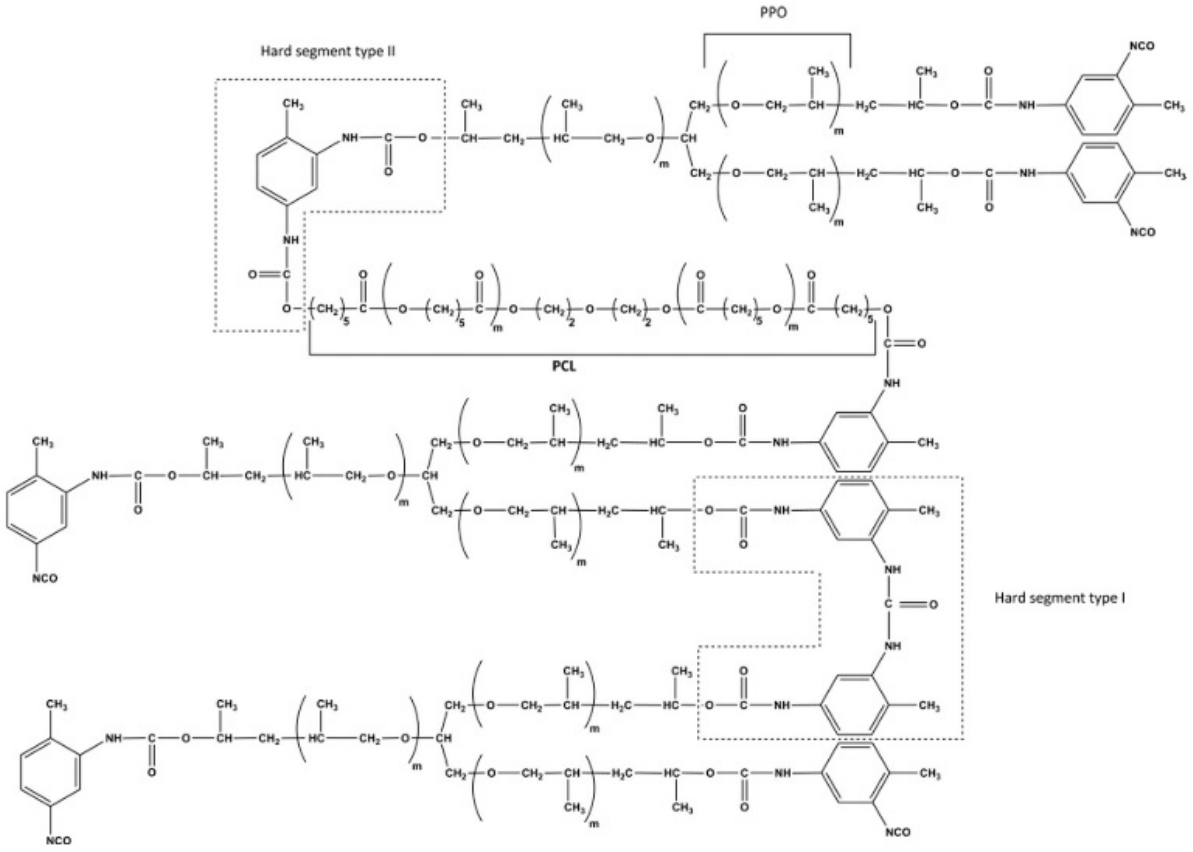

Figure 2.1: Example of the chemical structure of the poly(ester urethane urea) containing two types of SS's (PPO and PCL) and type I and II of HS's [9].

Previous studies showed that the variation of the ratio of PU to PCL diol content in the membrane formulation altered the surface energy, phase morphology, both in the bulk and near the surface, and affected hemocompatibility. The type, length and ratio of the different segments (SS and HS), their crystallizability, as well as the method of preparation also contributed to phase morphology and bulk and surface properties [13]. Plus, the increase of PCL diol content lead to smoother blood-contacting surfaces, more hydrophilic and with higher maximum zeta potentials. It is important to note that, more hydrophilic membranes are linked with lower platelet deposition and inhibition of extreme states of platelet activation [14].

Besteiro et. al [13] tested four nonporous PEUU membranes with different compositions varying PU/PCL ratio (100/0, 95/5, 90/10, 75/25). From these tests was concluded that the elastic modulus varied negligibly with membrane composition, values between 0.1-0.2 MPa, where the 95/5 membrane showed not only the highest elastic modulus but also the highest Ultimate Tensile Strength (UTS), implying that it may have the highest phase separation between HS and SS. In addition, concerning the phase morphology of the two Soft Segments in the bulk, the 90/10 membrane showed two glass transitions, while a single glass transition was observed in the Dynamic Mechanical Thermal Analysis (DMTA) thermograms for all the other membranes tested. Therefore, these results indicate that the two Soft Segments are immiscible with intermediate PCL-diol contents (10 wt.%) and miscible with the lowest and highest contents, which can be explained by the different degrees of flexibility and cross-linking, being the intermediate formulation the least flexible.

Regarding hemocompatibility, all membranes were nonhemolytic for a contact time with blood of 3

hours. Additionally, the absence of platelet adhesion was coincident with higher Hard Segment aggregation in the region near the surface and with mixing between the two Soft Segments in the bulk, given that 75/25 membrane, which showed higher Hard Segment aggregation, did not show platelet adhesion unlike the 90/10 [13].

Other studies carried out by de Pinho's research group [14], this time on integral asymmetric PEUU membranes, revealed that the contact angles on the top dense surfaces decreased from 71º to 66º, 63º and 59º when increasing the PCL-diol content from 0 wt.% to 5, 10 and 15 wt.%, respectively. Thus, the smallest contact angle corresponding to the highest content in PCL-diol exhibited a more hydrophilic surface, as opposed to the 0 wt.%.

Finally, the opposite pattern was observed for the extreme zeta potential values, where the highest PCL-diol content membrane (85/15) shows the highest result (12mV) while the least hydrophilic membrane has the lowest.

2.3 Phase Segregation and Gas Permeation Properties

For the nonporous membranes synthesized in the absence of PCL, studies showed only one type of SS (PPO) and one type of HS (two urethane groups linked by two toluene groups and one urea group), with a stoichiometric HS weight content of 20%. On the other hand, the remaining nonporous membranes synthesized with 5, 10 and 15 wt.% PCL-diol contained not only two types of SS (PPO and PCL) but also two types of Hard Segments, as shown in figure 2.1 above. One of the Hard Segments is identical to the one present in the first membranes, while the other is characterized by two urethane groups linked by one toluene group. For these membranes, stoichiometric total HS% of 16, 15 and 14%, respectively, were calculated [9].

Regarding the gas permeation, studies by Faria et. al [9] concluded that 10% PCL content membranes exhibit the highest CO_2 permeation followed by the 5% and 0%, opposing to the 15% that presents the lowest CO_2 permeation values. Plus, the permeability coefficients vary with PCL content and the results were 188, 250, 337 and 113 Barrer for 0, 5, 10 and 15%, respectively. For O_2, permeability coefficients don't vary significantly, remaining approximately constant for all the membranes. Diffusion coefficients for CO_2 increased in order of 5, 15, 0 and 10%.

Gas permeation characteristics of PUs are strongly dependent on the composition, type and molecular weights of the SS, HS/SS ratio and the degree of phase segregation between the two types of segments. PCL is also responsible for the formation of Hard Segment aggregates by the urethane groups, in the Soft Segment phase. The aggregation state increases with the increase of this component. In addition, besides being a polar gas facilitating the interactions with polar polymer chains, CO_2 has a smaller molecular size (penetrant kinetic diameter) [15] and a higher condensation temperature when compared with O_2, leading to permeability values 10-30 times higher, that are also related with greater solubilities in the membrane.

However, the synthesis of integrally skinned asymmetric membranes composed of a bottom porous surface and a thin dense blood-contacting surface brought up new ways of achieving higher gas permeation properties and a wide range of different surface morphologies. While the porous phase is known to promote plasma protein adsorption, platelet deposition and plasma leakage but also contribute to greater gas permeations, the thin dense layer prevents the blood to contact with this phase leading to the optimization of the process [16].

Faria et. al [17] synthesized integral asymmetric bi soft segment poly(ester urethane urea) through a novel procedure based on a modification in the casting solutions preparation step of the phase inversion technique. The two pre-polymers mentioned in the beginning of section 2.1 were dissolved in a mixture

of Dimethylformamide (DMF)/Diethyl Ether (DEE), varying the weight ratio over 11, 5 and 3 and the casting was carried out varying the solvent evaporation times as well (30s, 60s and 90s). From the studies performed in this membranes was concluded that with the increase of DEE concentration not only the thickness of the active layer decreased but the sublayers became more porous.

The measurements of the carbon dioxide and oxygen volumetric fluxes were performed at pressures between 76 cmHg to 380 cmHg and allowed the perception that by minimizing the thickness of the dense layer, the permeation rates of O_2 and CO_2 were enhanced. All the PU membranes exhibited experimental CO_2 permeances in the range required for membrane oxygenators. In opposition to the exposed results, the authors concluded that O_2 permeances still needed improvements [17].

Chapter 3

Framework and Thesis Objectives

Previous researches and studies presented in the literature revealed a great capacity given by Polyurethane membranes on applications in medical devices, as well as its ability to enhance the permeation properties and hemocompatibility when synthesized with two Soft Segments (PPO and PCL). Thus, the present work will be focused on the evaluation of different compositions in the gas permeations.

The main objectives of this thesis are:

1. Synthesis and optimization of nonporous and integrally asymmetric Poly(ester urethane urea) (PEUU) membranes with PCL as second Soft Segment and their characterization by Scanning Electron Microscopy (SEM);

2. Determination of the permeation properties of both nonporous and asymmetric Poly(ester urethane urea) (PEUU) membranes towards CO_2, O_2 and N_2;

Chapter 4

Mass Transport Phenomena through Dense Membranes

In nonporous membranes the main mechanism of transport is commonly explained by the solution diffusion mechanism. Thus, the transport of a gas, vapour or liquid through a dense membrane can be described in terms of a solubility (S) function, a thermodynamic parameter that measures the amount of penetrant sorbed by the membrane under equilibrium conditions, and diffusivity (D), as shown in equation 4.1.

$$\mathrm{P} = \mathrm{S}\,\mathrm{D} \tag{4.1}$$

where P is the permeability [18].

It is also known that, in steady-state, the diffusive flux in polymeric membranes obeys Fick's first law of diffusion:

$$\mathrm{J_i} = -\mathrm{D_i} \cdot \frac{\mathrm{dC_i}}{\mathrm{dx}} \tag{4.2}$$

where J_i represents the flux of species i, being the amount of said species passing in unit time through the unit area of section in the direction of the concentration gradient, dci/dx, and D_i is the diffusion coefficient.

Integrating Fick's first law over the total thickness of the membrane (δ), considering the following boundary conditions: (i) x = 0 on the upstream face (feed) and the penetrant concentration is equal to C_{i0}; (ii) x = δ on the downstream face (permeate) and $C_{i\delta}$ corresponds to the penetrant concentration on the permeate side, the flux can be written as equation 4.3 [18, 19].

$$\mathrm{J_i} = \frac{\mathrm{D_i}}{\delta} \cdot (\mathrm{C_{i0}} - \mathrm{C_{i\delta}}) \tag{4.3}$$

Studies show that the solubility of gases in elastomer polymers is very low and can be described by Henry's law, which makes it possible to consider that the gas diffusion coefficient is constant and does not depend on the concentration. On this note, Henry's Law states that the concentration inside the polymer is proportional to the applied pressure, for ideal systems, as shown in equation 4.4.

$$\mathrm{C} = \mathrm{S\,p} \Leftrightarrow \mathrm{S_i} = \frac{\mathrm{C_{i0}}}{\mathrm{p_f}} = \frac{\mathrm{C_{i\delta}}}{\mathrm{p_p}} \tag{4.4}$$

In this equation, both pressures p_f and p_p are known, being the feed and permeate pressure, respectively. Combining equations 4.3, 4.4 and keeping in mind the solution diffusion mechanism its possible

to obtain the expression exhibited below.

$$\mathrm{J_i} = \frac{\mathrm{S_i\,D_i}}{\delta} \cdot (\mathrm{p_f} - \mathrm{p_p}) = \frac{\mathrm{P_i}}{\delta} \cdot (\mathrm{p_f} - \mathrm{p_p}) \tag{4.5}$$

This relation shows that the diffusive flux is proportional to the pressure difference across the membrane, driving force of the system, and inversely proportional to the thickness, while the permeability is the proportionality constant which is commonly expressed in Barrer [18, 20].

$$\mathrm{Barrer} = 10^{-10} \left(\frac{\mathrm{cm^3\,cm}}{\mathrm{cm^2\,s\,cmHg}} \right) \tag{4.6}$$

In transient state, where the concentration does depend on the time, the transport process is then described by Fick's Second law, assuming the membrane is isotropic and Knudsen mechanism is controlling. For that reason, the simplifying assumption of constant diffusion coefficient (independent of distance, time and concentration) is possible if the pressures are kept low [20, 21].

$$-\frac{\partial \mathrm{C_i}}{\partial \mathrm{t}} = \frac{\partial \mathrm{J_i}}{\partial \mathrm{x}} \tag{4.7}$$

Substituting the flux parcel by Fick's First law, it is easy to obtain equation 4.8.

$$\frac{\partial \mathrm{C_i}}{\partial \mathrm{t}} = \mathrm{D_i} \cdot \frac{\partial^2 \mathrm{C_i}}{\partial \mathrm{x}^2} \tag{4.8}$$

Similarly to the previous demonstrations, the solution of Fick's Second law can be deducted applying the initial and boundary conditions listed below:

$$\text{(i)}\ \mathrm{C_i}\,(\mathrm{x}, 0) = 0 \tag{4.9a}$$

$$\text{(ii)}\ \mathrm{C_i}\,(0, \mathrm{t}) = \mathrm{C_{i0}} \tag{4.9b}$$

$$\text{(iii)}\ \mathrm{C_i}\,(\mathrm{x}, \mathrm{t}) = \mathrm{C_{i\delta}} \approx 0 \tag{4.9c}$$

meaning that if the initial concentration, C_{i0}, remains constant and $C_{i\delta}$ is approximately zero, the solution of equation 4.8 subjected to the boundary conditions by either Laplace transform or separation of variables is given below, eq. 4.10.

$$\mathrm{Ci} = \mathrm{C_{i0}} \cdot \left(1 - \frac{\mathrm{x}}{\delta}\right) + 2 \cdot \frac{\mathrm{C_{i0}}}{\pi} \times \sum_{\mathrm{n}=1}^{\infty} \frac{1}{\mathrm{n}} \cdot \sin\left(\frac{\mathrm{n\,\pi\,x}}{\delta}\right) \cdot exp\left(-\frac{D_i\, n^2\, \pi^2\, t}{\delta^2}\right) \tag{4.10}$$

The diffusive flux, J_i, can be obtained applying Fick's law in the concentration profile present in eq. 4.10, as the expression 4.11 exposes.

$$\mathrm{J}\,(\mathrm{x}, \mathrm{t}) = \frac{\mathrm{D_i\,C_{i0}}}{\delta} + 2 \cdot \frac{\mathrm{D_i\,C_{i0}}}{\delta} \times \sum_{\mathrm{n}=1}^{\infty} \cos\left(\frac{\mathrm{n\,\pi\,x}}{\delta}\right) \cdot exp\left(-\frac{D_i\, n^2\, \pi^2\, t}{\delta^2}\right) \tag{4.11}$$

where the second term in the flux equation represents the transient contribution and the first term is the steady state portion of the flux. It is a function of time and displacement in the direction of diffusion and hence can be solved for the fluxes entering and leaving the membrane (x = 0 and x = δ, respectively). Integration of the general flux equation, Eq. 4.11, fixing x= δ, with respect to time, yields the amount permeating out of the membrane. The permeate pressure then, subject only to the boundary condition restrictions, is obtained from the amount permeating through the end of the membrane, leading to

equation 4.12.

$$\mathrm{p_p} = \frac{\mathrm{A\,D_i\,p_f}}{\mathrm{V}\,\delta} \cdot \left[t - \frac{\delta^2}{6\,D_i} + \frac{2\,\delta^2}{\pi^2\,D_i} \times \sum_{n=1}^{\infty} \frac{(-1)^{n+1}}{n^2} \cdot exp\left(-\frac{D_i\,n^2\,\pi^2\,t}{\delta^2} \right) \right] \tag{4.12}$$

where A is the cross-sectional area available for gas phase penetration perpendicular to the direction of diffusion and V is the volume of the receiving chamber. Minding the steady state assymptote, taking the limit as t $\rightarrow \infty$, the transient summation terms are reduced to zero and the downstream pressure rise is given by eq. 4.13.

$$\lim_{\mathrm{x}\to\infty} \mathrm{p_p\,(t)} = \frac{\mathrm{A\,D_i\,p_f}}{\mathrm{V}\,\delta} \cdot \left(\mathrm{t} - \frac{\delta^2}{6\,\mathrm{D_i}} \right) \tag{4.13}$$

Lastly, the plot of flux versus time in conjunction with the plot of the asymptotic linear permeation flow, in steady state, results in an intercept on the time axis that is the time lag denoted by t_{lag} and given by the following equation.

$$\mathrm{t_{lag}} = \frac{\delta^2}{6\,\mathrm{D_i}} \tag{4.14}$$

This parameter is obtained from the finite time difference observed between the time at which the penetrant enters the membrane and the time at which the flow rate of diffusing species into the closed volume reaches a steady state of permeation. It also represents transient or dynamic component [21, 22].

Furthermore, the ideal selectivity of the membrane, α, can be determined by the ratio of the permeabilities or permeances of the individual gases. Thus, for a mixture of gases A and B, the ideal selectivity is defined as [20]:

$$\alpha_{\mathrm{A/B}} = \frac{\mathrm{Perm_A}}{\mathrm{Perm_B}} = \frac{\mathrm{P_A}}{\mathrm{P_B}} \tag{4.15}$$

Chapter 5

Experimental

5.1 Materials

5.1.1 Synthesis of Poly(ester urethane urea) Membranes

As mentioned before, Poly(ester urethane urea) membranes can have one or two types of Soft Segments in their constitution, if they are synthesized without or with PCL. On that note, for the preparation of the said membranes two prepolymers were used: Poly(propylene oxide) (PPO) based Polyurethane prepolymer (PUR) with three isocyanate terminal groups and molecular weight of 3500 Da, provided by Fabrires-Produtos Químicos, SA, and Poly(caprolactone) diol prepolymer with a molecular weight of approximately 530 Da, supplied by Sigma-Aldrich, being the chain extending prepolymer. Both chemical structures of the two prepolymers are shown in figure 5.1.

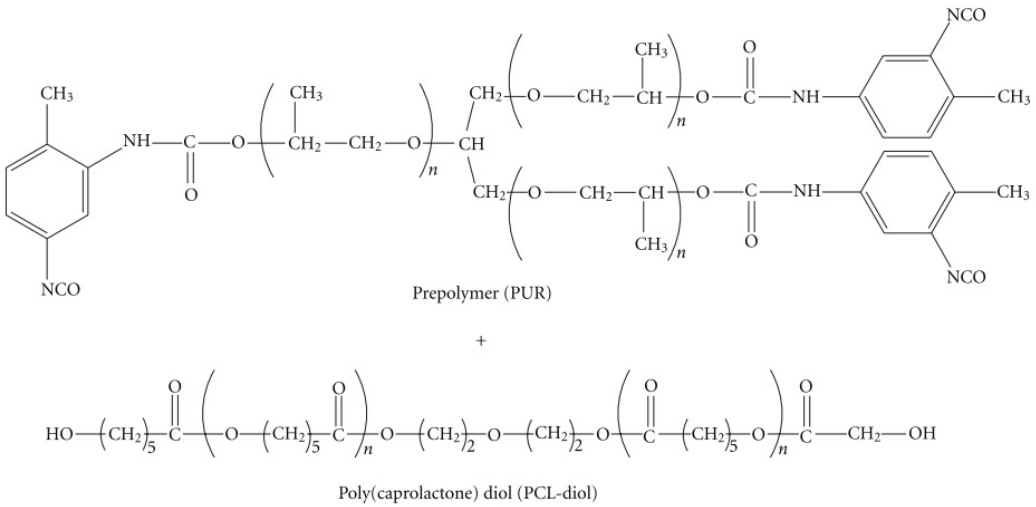

Figure 5.1: Chemical Structures of the two prepolymers: PUR and PCL diol [14].

In terms of Hard Segments, when in absence of PCL only one type of chemical structure is present, designated as type I. Type I is originated by the reaction of two PUR segments consisting of two urethane groups linked by two toluene groups and one urea group (figure 5.2).

The effect of adding PCL can then result in the formation of two distinct structures, as it was previously shown in figure 2.1 [9]: Type I and also Type II, created by the reaction of a PUR segment with a PCL segment consisting of two urethane groups linked by a toluene group. This type is shorter than type I.

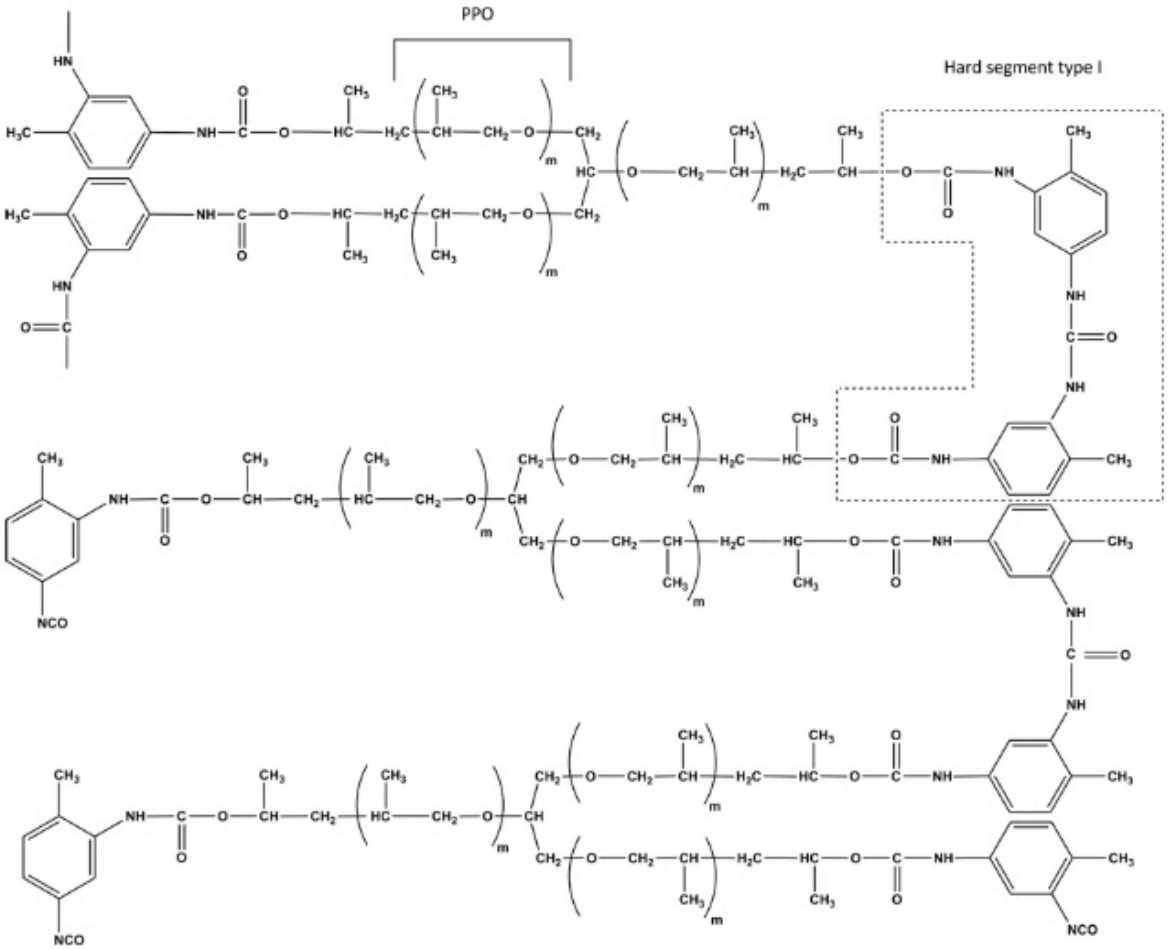

Figure 5.2: Example of the chemical structure of the poly(urethane urea) containing one type of SS (PPO) and type I HS's [9].

Regarding the solvents, the synthesis was performed using Dimethylformamide (DMF) (w/w% grade, 99.8%) and Diethyl Ether (DEE) (w/w% grade, 99.5%) both supplied by Panreac. As a catalyst Tin(II)-ethylhexanoate (wt.% 95%) from Sigma-Aldrich was used.

5.1.2 Gases

Gas permeation tests were performed using gases provided by Air Liquid, more specifically, oxygen (purity $\geq$ 99.5%), carbon dioxide (purity $\geq$ 99.98%) and nitrogen (purity $\geq$ 99.999%).

5.2 Synthesis of Nonporous Poly(ester urethane urea) Membranes

For the preparation of nonporous Poly(ester urethane urea) membranes, the content of PCL was varied and a simple solvent evaporation method was adopted. The variation of this prepolymer generates structures identical to the ones present in figures 2.1 and 5.2.

To start the preparation it is necessary to make the casting solutions. These casting solutions are composed by the PUR prepolymer plus the two solvents (DMF and DEE) and the Tin(II)-ethylhexanoate catalyst, if the goal is to obtain membranes with only one of the Soft Segments, otherwise it is mandatory to add the second prepolymer, PCL-diol. Next, said solutions are left under agitation for approximately 2

hours, at room temperature. It is important to state that the DMF/DEE and polymer/solvent ratios were kept constant and equal to 3/1 and 65/35 wt.%, respectively, throughout the studies.

Secondly, the casting solutions were poured into a 250 μm casting knife, which were then spread on a glass plate. Films were left to dry at room temperature for a minimum time of 24 hours.

Lastly, the membranes were washed with deionized water, detached carefully from the glass plates and layed on paper sheet.

Synthesized membranes' names obeyed a specific format being PUX, where X refers to the wt.% of PCL. Therefore, the designations given were PU0, PU5, PU10 and PU15, corresponding to 0%, 5%, 10% and 15% of PCL content, respectively, as shown in table 5.1.

Table 5.1: Designations and chemical compositions of PU membranes synthesized by varying PCL content.

Membrane	**PUR/PCL (wt.%)**
PU0	100/0
PU5	95/5
PU10	90/10
PU15	85/15

5.3 Synthesis of Integral Asymmetric Poly(ester urethane urea) Membranes

In case of the preparation step of asymmetric Poly(ester urethane urea) membranes, a modified version of the phase inversion technique was used instead [23, 24], varying also the PCL content in each casting solution but maintaining a solvent evaporation time of 1, 5 and 10 minutes. As mentioned above, the structures may vary between the ones present in figures 2.1 and 5.2 with the variation of the prepolymer.

To begin the synthesis it was necessary to prepare the casting solutions, as well. The same casting solutions explained on section 5.2 were used, meaning that all ratios between prepolymers and solvents were kept equal to the previous membranes.

Similarly, in a second phase of the preparation step of integrally asymmetric membranes, the casting solutions were poured into a 250 μm casting knife and then spread on a glass plate. After fulfilling the evaporation time set for each case, the plates were submerged in a coagulation bath filled with deionized water where remained for about 12 hours.

In the end, when removed from the bath, the membranes were gently taken out of the glass plates, placed over a paper sheet and left to dry at room temperature, as performed before on the nonporous.

Synthesized membranes' names obeyed a specific format being PUX-Y, where X refers to the wt.% of PCL and Y to the solvent evaporation time. Therefore, membranes with 1 minute of solvent evaporation were designated by PU5-1, PU10-1 and PU15-1, the ones with 5 minutes by PU5-5, PU10-5 and PU15-5, and lastly for the 10 minutes of solvent evaporation time membranes were given the designations of PU5-10, PU10-10 and PU15-10, as summed up in table 5.2.

Table 5.2: Designations, chemical compositions and solvent evaporation times of PU membranes synthesized by varying PCL content.

Membrane	PUR/PCL (wt.%)	Solvent Evaporation Time (min)
PU5-1	95/5	1
PU10-1	90/10	1
PU15-1	85/15	1
PU5-5	95/5	5
PU10-5	90/10	5
PU15-5	85/15	5
PU5-10	95/5	10
PU10-10	90/10	10
PU15-10	85/15	10

5.4 Membrane characterization by Scanning Electron Microscopy (SEM)

All the synthesized membranes were observed by Scanning Electron Microscopy (SEM) using a Hitachi S-2400 SEM microscope (Hitachi, Tokyo, Japan). For the observation, multiple samples were prepared by fracturing parts of the specific membrane after being freezed with liquid nitrogen. These small pieces were then mounted on a stub and sputter-coated with gold. Images of the top, cross-sections and bottom surfaces for each sample were taken.

5.5 Gas Permeation Setup and Tests

Gas permeation tests were performed in a setup built by Eusébio, T. [25]. Later, the same setup was optimized by Pon, G. [26] allowing the elimination of problems such as low reproducibility and high uncertainty associated for more permeable membranes. The transient state was then possible to observe not only in measurements with CO_2 but with O_2 and N_2 as well, enabling the determination of the diffusion and solubility coefficients for these gases by the time lag method.

The setup was designed including a vacuum pump to make sure the system was gas free before any measurement, obeying the initial and boundary conditions applied in the Fick's Second Law of diffusion, since the goal was to obtain more precise gas permeation measurements of membranes.

Furthermore, the final apparatus consists of a permeation cell, a Feed Pressure Sensor (PfT) (Setra, Model 205, Massachusetts, USA), a Permeate Pressure Transmitter (PpT) (Intelligent Transmitter Paroscientific, Series 6000, model 6100A-CE Inc. Washington, USA) attached to a Paroscientific model 710 display unit, which is connected to a computer, a small cylinder with a volume of 12.6 ± 0.1 cm^3 (Cylinder 1) and a big cylinder with a volume of 167.2 ± 0.2 cm^3 (Cylinder 2). Lastly, the tubing system in the receiving chamber has a volume of 13.5 ± 0.01 cm^3, composed by tubes of stainless steel 316 with an external diameter of 1/8 inch (Hoke®), needle valves (3700 Series, Hoke®) and tube fittings made of stainless steel, titanium and brass (Gyrolok®). The total volume of the permeate side is 193.3 ± 0.3 cm^3.

It is important to note that both cylinders and tubes were calibrated prior to the measurements, where the first cylinder calibration was done by gravimetry, while the second plus the tubes were done by gas expansion [26].

Concerning the permeation cell itself, the membrane is placed between two plates of stainless steel with an active surface area of 9.62 cm^2. A schematic representation of the cell is shown in the figure below.

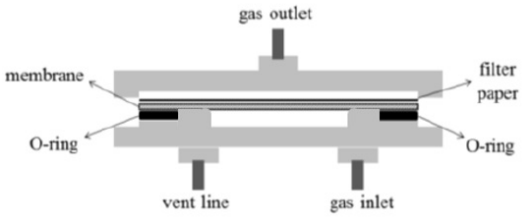

Figure 5.3: Schematic representation of the permeation cell.

The equipment was installed in a thermostatic system (air bath) which consists of a wine fridge (cold source), a resistance thermometer, a heater connected to a PID controller and a fan to homogenize the inner temperature. The variation of the pressure was recorded with the software Digiquartz® version 2.0 (Paroscientific Inc, Washington, USA).

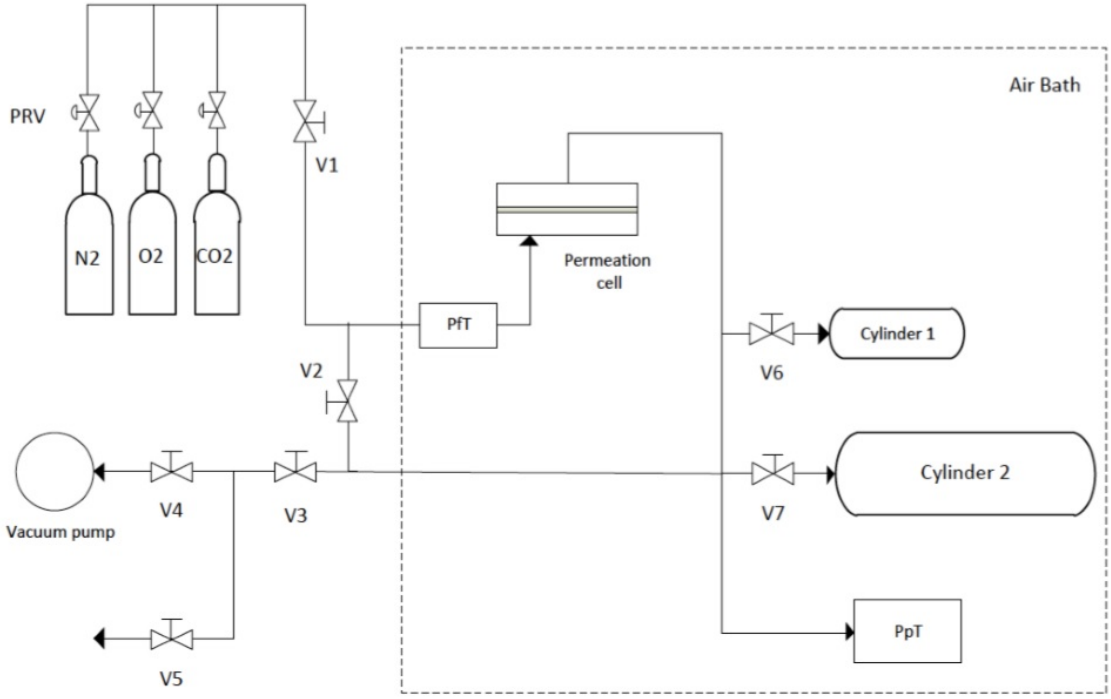

Figure 5.4: Schematic representation of the gas permeation Setup [26].

To initiate the measurement, the setup must be thermostated. When a temperature of approximately 37±0.2 °C is reached, the system is ready to start measuring. After, valves V2 and V3 must be closed, maintaining the vacuum provided by the pump. Secondly, the pressure of the gas being fed (O_2, CO_2 or N_2) has to be regulated on the pressure reducing valve (PRV) in the gas cylinder, while valve V1 is closed. Finally, valve V1 can be opened and permeation begins to be recorded as a function of time by the PpT sensor.

Once the membrane is inserted in the cell, it is possible to determine the gas flux through it by monitoring the variation of pressure with time. During the experiment, the value given by the PfT must be checked to make sure its value is constant throughout the test.

In the end, the reverse process is adopted by closing valve V1 and opening valves V2 and V3, ensur-

ing that the setup is completely degassed before the next measurement. It is important to mention that valve V5 is always closed, except when there is the need to return to atmospheric pressure, and valves V6 and V7 are opened or closed depending on the gas that is being measured due to the sensitivity of the system. Thus, permeation measurements of oxygen and nitrogen were carried out with both valves V6 and V7 closed, which corresponds to a volume of 13.5 cm^3, while for carbon dioxide both valves were opened making up a volume of 193.3 cm^3.

From the data collected by every test, the average permeances, diffusion and solubility coefficients were calculated for the nonporous membranes, as well as the average permeances for the integral asymmetric ones.

Chapter 6

Results and Discussion

6.1 Surface and Cross-section characterization of Poly(ester urethane urea) nonporous membranes by SEM

Samples of the nonporous membranes prepared with 0, 5, 10 and 15 wt.% PCL, DMF/DEE and polymer/solvent ratios of 3/1 and 65/35 wt.% were observed by Scanning Electron Microscopy, having obtained the images presented in figure 6.1.

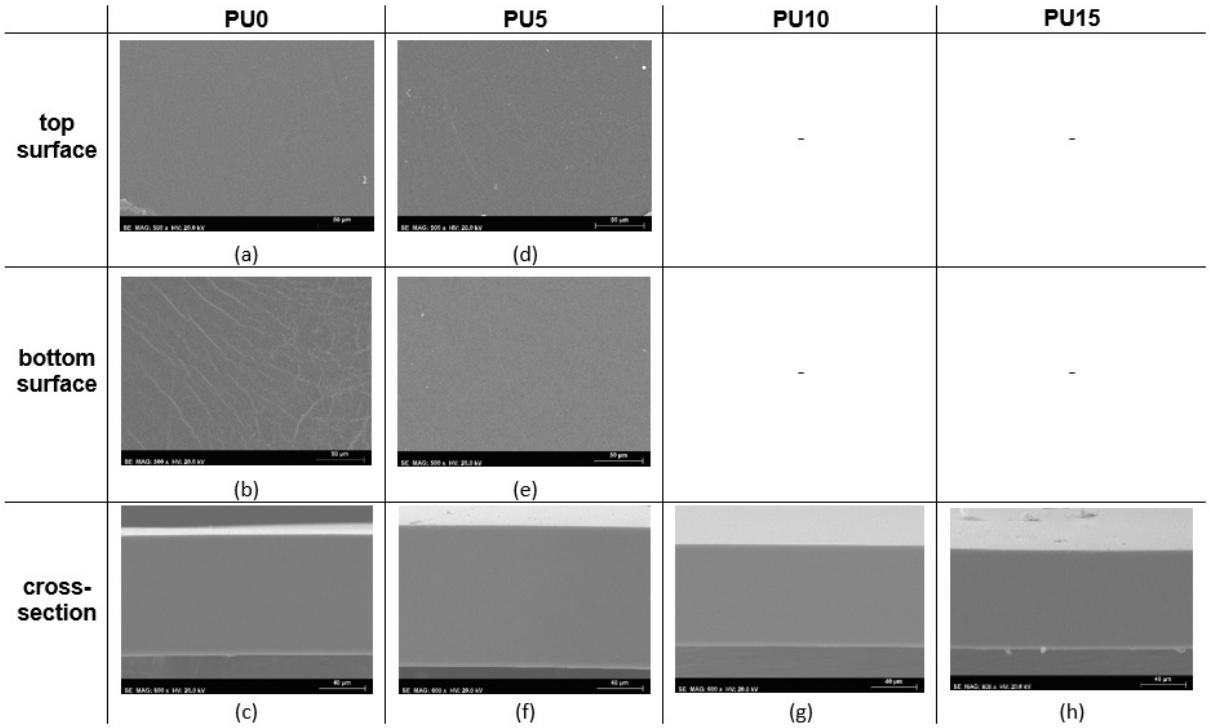

Figure 6.1: Images of the top/bottom surfaces and cross-sections obtained by SEM: (a) top surface, (b) bottom surface and (c) cross-section of membrane PU0; (d) top surface, (e) bottom surface and (f) cross-section corresponding to membrane PU5; (g) and (h) cross-sections of membranes PU10 and PU15, respectively.

Observing the images shown above, it is possible to confirm that all the compositions studied result in totally dense membranes once there is no sign of any visible pores. Cross-sections show also the symmetrical character of these membranes. When ready to use, said membranes are transparent, very sticky and slightly elastic.

The average total membrane thickness was determined from four different measurements in each sample using a digital caliper. Table 6.1 presents these values as well as the respective standard deviations.

Table 6.1: Average thicknesses and respective standard deviations for nonporous membranes PU0, PU5, PU10 and PU15.

Membrane	**Thickness, δ (mm)**
PU0	0.112$\pm$0.006
PU5	0.115$\pm$0.004
PU10	0.107$\pm$0.004
PU15	0.112$\pm$0.001

Observing the results of the measurements performed manually and comparing with the images obtained through SEM, it is possible to notice a greater membrane thickness for an intermediate composition of 5% PCL, in both cases. In addition, there was a slight decrease in thickness from the membrane without the second prepolymer to the two membranes with larger quantities, which was not reflected in the measurements made with the digital caliper.

6.2 Gas Permeation Experiments - Nonporous Poly(ester urethane urea) membranes

To evaluate gas permeation on the membranes synthesized and observed by SEM, several experiments were run applying a constant volume method where the pressure evolution was recorded, using the apparatus described in section 5.5. The tests were performed with multiple feed pressures.

Each experiment gives back a permeation curve which consists on the evolution of the pressure on the permeate side as a function of time (figure 6.2). Similar curves were obtained for all 4 membranes at different feed pressures.

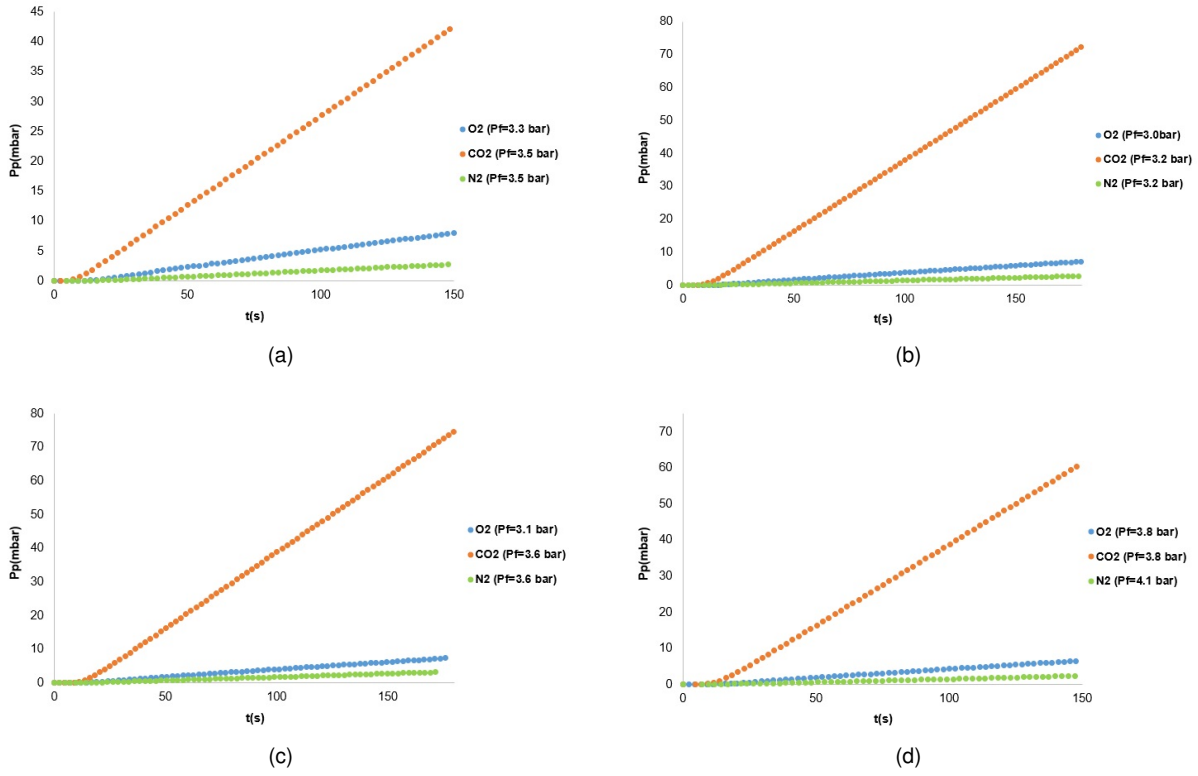

Figure 6.2: Permeation curves of gases O_2, CO_2 and N_2 for membranes (a) PU0, (b) PU5, (c) PU10 and (d) PU15.

From figure 6.2 is possible to acknowledge the presence of two distinct zones in every curve: the first and constant corresponding to the transient state and the second, where a progressive increase of pressure is registered, the steady state. Also, a clear conclusion to take is that, for similar feed pressures, the slope of the steady state increases in order of N_2, O_2 and CO_2, as seen before by Pon, G. [26].

Moreover, the slope (dp_p/dt) of every steady state zone enables the calculation of a volumetric flux, J. To start the calculations it is necessary to convert the slope in a volumetric flow, dV/dt. Thus, the Ideal Gas Law is applied first, obtaining a molar flow, dn/dt:

$$\frac{\mathrm{d}n}{\mathrm{d}t} = \frac{\mathrm{d}p_p}{\mathrm{d}t} \cdot \frac{V_s}{RT} \tag{6.1}$$

where V_s is the volume of the receiving chamber, R is the ideal gas constant and T is the absolute temperature at which the experiments were performed. It is important to note that the application of the Ideal Gas Law is a good approximation to experimental conditions, since the experiments were carried

out at low pressures, as well as relatively high temperatures.

Subsequently, to convert the previous result given by equation 6.1 into a volumetric flow in STP conditions, the procedure explained in expression 6.2 is adopted.

$$\frac{\mathrm{d}V}{\mathrm{d}t} = \frac{\mathrm{d}n}{\mathrm{d}t} \cdot \frac{RT_{STP}}{p_{STP}} = \frac{\mathrm{d}p_p}{\mathrm{d}t} \cdot \frac{V_s T_{STP}}{T p_{STP}} \tag{6.2}$$

In this expression, T_{STP} and p_{STP} represent the temperature and pressure in STP conditions, which are 273.15 K and 1 atm.

Lastly, the computation of the volumetric flux is achieved by dividing the volumetric flow by the effective membrane area, A.

$$J = \frac{\mathrm{d}V}{\mathrm{d}t} \cdot \frac{1}{A} \tag{6.3}$$

Once the fluxes were determined, it was possible to draw plots of this variable as a function of the Transmembrane Pressure (TMP). In the experiments executed, the TMP was obtained by the difference between the feed pressure, p_f, and the initial permeate pressure, p_{pi} (TMP=(p_f-p_{pi})). In the present cases, since the system was placed under vacuum before the beginning of every test, the value of the later variable is equal to 0.

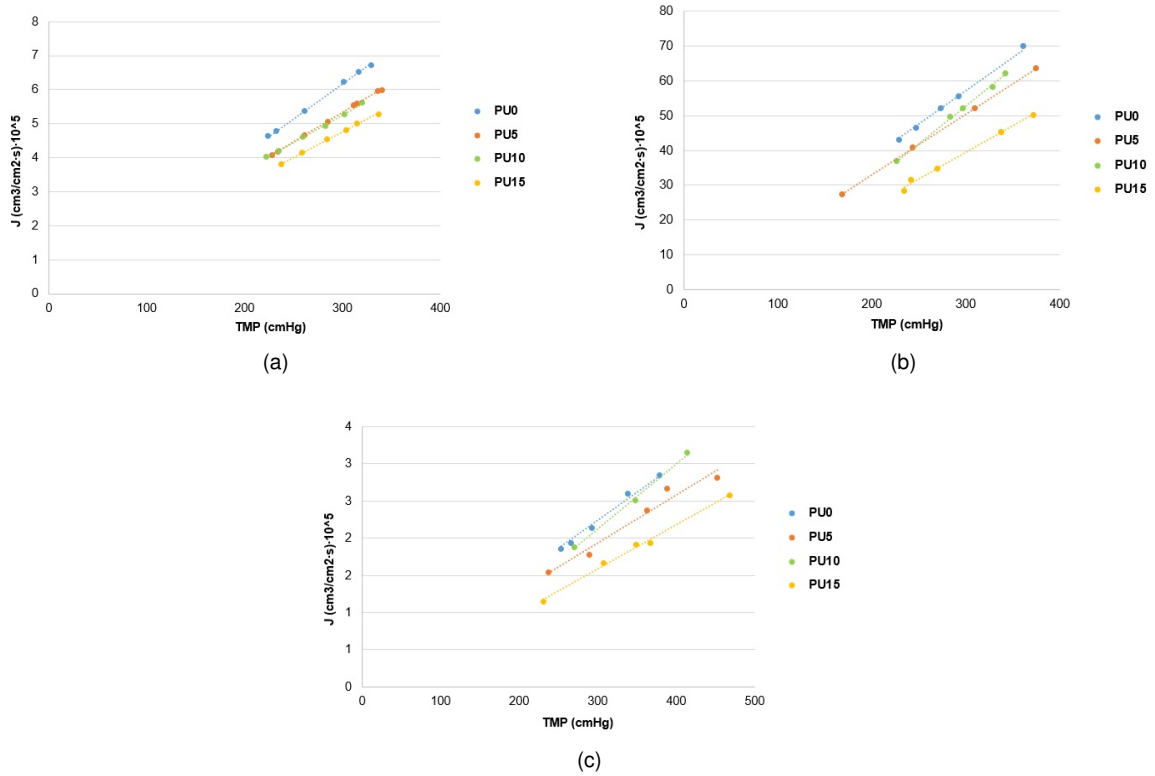

Figure 6.3: Volumetric fluxes as a function of TMP: (a) O_2, (b) CO_2 and (c) N_2.

Putting together the conclusions collected from figure 6.2 and observing figure 6.3, would be expected not only an increase of the fluxes of permeation in order of N_2, O_2 and CO_2, but also a linear relationship between the two variables involved tending to the point (0,0), meaning that for a transmembrane pressure of 0 cmHg the flow through the membrane is equal to 0 cm^3/cm^2s, which was visible in the plots. It is also important to note that the highest fluxes were obtained for PU0 while the lowest were observed for PU15.

Having now in mind the behavior of the fluxes as functions of TMP for all 4 membranes studied, from the slopes of the said plots, it was possible to calculate the permeances, $perm$:

$$perm = \frac{\mathrm{d}J}{\mathrm{d}(TMP)} \left[\frac{cm^3(STP)}{cm^2\, s\, cmHg} \right] \tag{6.4}$$

Due to the fact that this values greatly depend on the thickness of the membranes and since it varied from sample to sample, the permeances were converted to permeability coefficients to facilitate the comparison between results. On that note, the expression presented below was applied to all of the slopes.

$$P = perm \times \delta \times 10^{10} \tag{6.5}$$

where P is the permeability coefficient in Barrer units.

Knowing the thickness of all the samples, the average permeability coefficients determined are reported in table 6.2 and figure 6.4. The standard deviation values presented in the table were determined based on the calculation of two different permeability values from two distinct gas permeation tests, each one with a respective deviation. Thus, it corresponds to a rough estimate of the error.

Table 6.2: Average permeability coefficients obtained for N_2, O_2 and CO_2, using nonporous membranes PU0, PU5, PU10 and PU15.

	P (Barrer)		
Membrane	N_2	O_2	CO_2
PU0	9.9	22.9±0.4	230±0
PU5	7.4	20.1±0.3	198.3±1.3
PU10	10.1	18.2±0.4	218.0±36.1
PU15	6.7	16.5±0.5	168.1±0.5

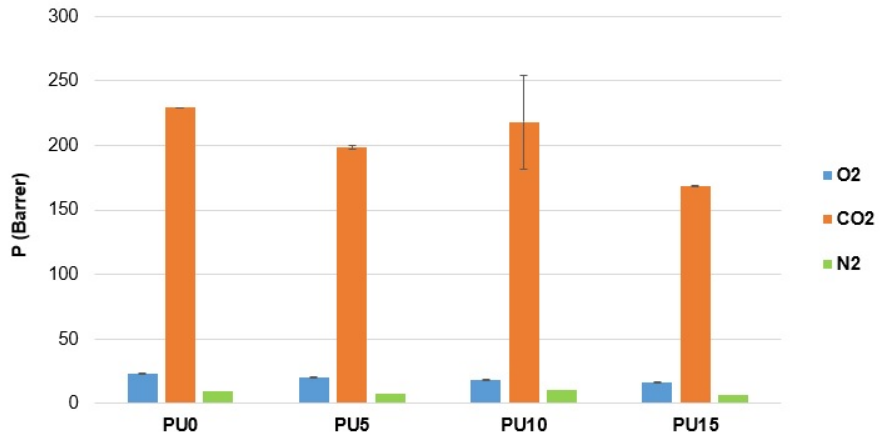

Figure 6.4: Average permeability coefficients obtained for N_2, O_2 and CO_2, using nonporous membranes PU0, PU5, PU10 and PU15.

Regarding the results obtained in the experiments, by analyzing the table and respective figure above, it is clear that the permeability coefficients for the oxygen are decreasing with the increase in PCL content. However, N_2 and CO_2 values did not obey the previous tendency. Overall, membrane PU0 showed the highest values of permeability, except for nitrogen.

Studies carried by Faria et. al [9] revealed that the CO_2 permeability coefficients varied with PCL content and were 188 Barrer for 0%, 250 Barrer for 5%, 337 Barrer for 10% and, finally, 113 Barrer for

15%. This tendency is observed also in the results shown in table 6.2 above, except for the membrane with less wt.% in PCL. On the other hand, values from the present work are slightly lower for membranes with 5% and 10% PCL opposing to the 0% and 15% ones being higher than expected. Additionally, was verified that P_{CO_2} values were 10-30 times higher than P_{O_2}, as previously estimated, but did not vary significantly with PCL content (10-11 Barrer).

Moreover, results gathered by Pon, G. [26] showed lower P_{CO_2} and higher P_{O_2} values to the 10% PCL membrane (208 Barrer and 21 Barrer, respectively), as well. It is important to note that these values were determined using the same PUR prepolymer and the same membrane preparation technique, contrary to the study carried out by Faria et. al. It is also important to mention that the thicknesses used in this study were significantly higher.

Comparing with other existing membranes used for artificial lungs, for example, Polypropylene (PP) and Polymethylpentene (PMP), permeability coefficients present values of 2-2.2 Barrer and 30-32.3 Barrer for P_{O_2} and 9-9.2 Barrer and 90-92.6 Barrer for P_{CO_2}, respectively. On that note, it can be affirmed that nonporous Poly(ester urethane urea) represent an improvement in gas permeability for both gases [27, 28]. However, it is important to keep in mind that the studies carried out in this work were performed in a gas/membrane/gas setup and not in a gas/membrane/liquid system, as the ones mentioned above. Thus, the resistance imposed to gas transport is higher and for that reason it is plausible to admit that the permeance values obtained in this work could be equivalent to those stated for existing artificial lungs.

In order to complete the study of permeabilities, ideal selectivities were also computed applying equation 4.15. Results are presented in table 6.3.

Table 6.3: Ideal selectivities and respective standard deviations for nonporous Poly(ester urethane urea) membranes.

	α		
Membrane	**O_2/N_2**	**CO_2/N_2**	**CO_2/O_2**
PU0	2.31±0.04	23.13±0.0	10.02±0.18
PU5	2.71±0.05	26.77±0.17	9.89±0.18
PU10	1.80±0.04	21.54±3.57	11.99±2.00
PU15	2.46±0.07	25.01±0.07	10.17±0.31

Results reported in both tables 6.2 and 6.3 shown that higher permeabilities correspond to lower selectivities for carbon dioxide, which is confirmed by previous studies [29].

Finally, an ANOVA test was executed to permeability results reported above. In particular, this test determines what is the probability that all data groups are the same, i.e, if the differences between different groups are due to our actions, differences within groups are what we expect of differences between data or are simply caused by the noise or variability. Therefore, was proved that, for a confidence level of 95%, there is a significant difference between the mean values.

6.2.1 Determination of the Total Surface Area required

As specified in section 1, the ideal oxygenator must be capable of performing an efficient gas exchange and, at the same time, should be gentle to the blood. Thus, the oxygenator must deliver about 250 cm^3 (STP)/min O_2 and remove about 200 cm^3 (STP)/min CO_2 [4].

It is known that the current normal membrane surface area required by an artificial lung lies between 2.5 to 6 m^2, or even lower when it comes to membranes oxygenators used for young children (0.25 m^2) [27, 28].

The surface areas were then estimated to meet said specifications for all four membranes by extrapolating the flux value for a pressure of 2.0 bar, based on the graphs in the figure 6.3 (table 6.4). This computation was only possible due to the linear nature of the relationship between flux and transmembrane pressure.

Table 6.4: Membrane surface areas estimated to meet specifications of oxygenators and respective volumetric fluxes.

	J $\times$ 10^{-5} (cm^3/cm^2s)		**Surface Area (m^2)**	
Membrane	O_2	CO_2	O_2	CO_2
PU0	3.1	28.6	13.5	1.2
PU5	2.7	25.3	15.7	1.3
PU10	2.6	26.4	15.8	1.3
PU15	2.4	19.7	17.5	1.7

As expected, higher fluxes of gas passing through the membrane are associated to lower transfer areas.

Additionally, as discussed before by Pon, G. [26], the improvements verified on permeability coefficients for carbon dioxide resulted in smaller surface areas required to execute the correct gas exchange. On the other hand, for oxygen, it would require a total membrane surface area of approximately 13 to 17 m^2 which is an order of magnitude higher than the average membrane surface area of commercial oxygenators.

6.2.2 Determination of Diffusion and Solubility Coefficients

Gas permeation experiments also allowed the determination of diffusion and solubility coefficients through further analysis of the permeation curves. Calculations were based on the time lag method (equation 4.14). The practical application of this method consists on tracing the steady state asymptote and determine its interception with the x axis (time axis). The x value of said interception its called time lag.

For every permeation curve, a procedure as shown on figure 6.5 was adopted. Later on, knowing the several time lag values, diffusion coefficients were obtained. Results are synthesized in table 6.5.

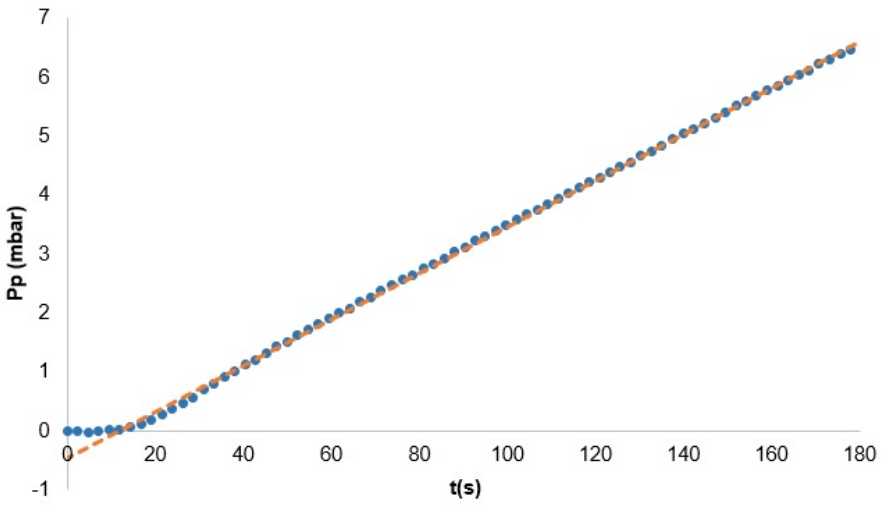

Figure 6.5: Example of the procedure adopted when determining the time lag, performed on a O_2 permeation curve for PU10 membrane.

Table 6.5: Average diffusion coefficients and respective standard deviations for nonporous membranes: PU0, PU5, PU10 and PU15.

	$\mathbf{D \times 10^{-6}\ (cm^2/s)}$		
Membrane	N_2	O_2	CO_2
PU0	1.40±0.05	2.14±0.44	1.66±0.15
PU5	1.22±0.11	1.91±0.16	1.63±0.15
PU10	1.22±0.14	1.59±0.20	1.36±0.08
PU15	1.00±0.02	1.74±0.12	1.42±0.08

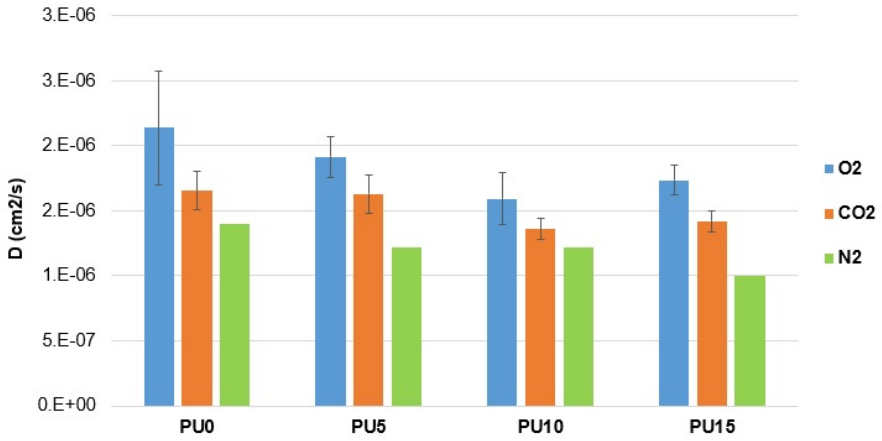

Figure 6.6: Average diffusion coefficients and respective standard deviations for nonporous membranes: PU0, PU5, PU10 and PU15.

Analysing the results given on table 6.5, it appears to reveal a tendency which is a decrease of diffusion coefficients from PU0 to PU10, for the three gases. For membrane PU15, although this variable increases again, it is always lower than the values obtained for PU0 and PU5, except for N_2 where D assume the lowest result registered.

Additionally, it would be expected that the diffusion coefficients increase in order of N_2, O_2 and CO_2 once the size of the gas molecules decreases in that order (3.64 Å, 3.46 Å and 3.30 Å, respectively) [29, 30]. However, instead of the tendency mentioned above, variable D increased in the order of N_2, CO_2 and O_2. A possible explanation is the fact that carbon dioxide is considered to be an interacting gas, while oxygen and nitrogen are non-interacting gases, increasing resistance to diffusion [31].

Starting from the values reported in table 6.5, solubility coefficients were easily obtained applying expression 4.1. Table 6.6 summarizes the average solubility coefficients and respective standard deviations for nonporous Poly(ester urethane urea) membranes.

Table 6.6: Average solubility coefficients and respective standard deviations for nonporous membranes: PU0, PU5, PU10 and PU15.

	$\mathbf{S \times 10^{-4}\ (cm^3/cm^3cmHg)}$		
Membrane	N_2	O_2	CO_2
PU0	7.07±0.24	11.13±1.68	140.01±11.80
PU5	6.14±0.60	10.64±0.93	123.25±12.92
PU10	8.40±1.00	11.86±2.14	160.03±8.50
PU15	6.74±0.16	9.62±1.21	119.22±7.38

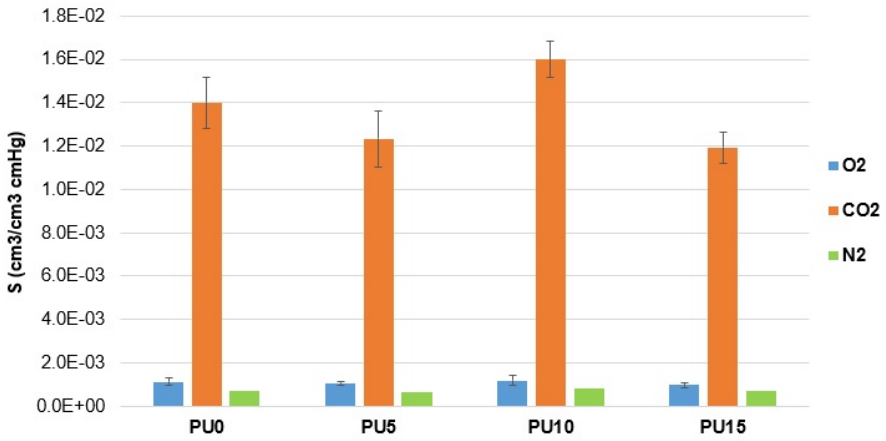

Figure 6.7: Average solubility coefficients and respective standard deviations for nonporous membranes: PU0, PU5, PU10 and PU15.

Solubility is greatly controlled by the ease of condensation of the gas molecules [31]. On that note, keeping in mind that the boiling points increase in order of N_2, O_2 and CO_2 [30], the latter is the most likely condensate. Moreover, it is noteworthy to mention that the work temperature used during the gas permeation tests (37ºC) is very close to the critical point of carbon dioxide, which is 31.1ºC. The remaining two gases present critical temperatures below 0ºC, meaning that even if the temperature is maintained and the pressure is greatly increased, the condensation of both gases will be impossible to achieve [30]. Results obtained on the presented experiments verify this fact since higher solubilities were registered for carbon dioxide, followed by oxygen and, finally, nitrogen.

As observed before for permeability results for N_2 and CO_2, experiments did not reveal a direct tendency between solubility coefficient values as the PCL content was varied. More specifically, PU10 always showed higher values when compared to other wt.%, followed by PU0, while PU15 exhibited the lowest solubility coefficients, except for N_2.

The present determined results can be compared with the previous study performed for carbon dioxide where results for the diffusion coefficient exhibited values of $5.86 \times 10^{-7} cm^2/s$, $2.21 \times 10^{-7} cm^2/s$, $8.15 \times 10^{-7} cm^2/s$ and $4.64 \times 10^{-7} cm^2/s$ for membranes with 0%, 5%, 10% and 15% PCL, respectively. Regarding solubility coefficients, values of $3.22 \times 10^{-2} cm^3/cm^3 cmHg$, $11.30 \times 10^{-2} cm^3/cm^3 cmHg$, $4.14 \times 10^{-2} cm^3/cm^3 cmHg$ and $2.44 \times 10^{-2} cm^3/cm^3 cmHg$ were determined, for the same order of membranes [9]. Comparing all values reported above, it was possible to note that for both variables D and S no tendency was evidenced on the study also. Furthermore, every diffusion coefficient value determined on this work is higher than the ones found on the study, while solubility is always lower.

Overall, since it is a process controlled by solubility, that is, an increase in solubility will have a greater impact than an increase in the diffusion coefficient, the low permeability registered for N_2 when compared to O_2 and CO_2 can be explained and supported by the low solubility, reflected in low diffusion. Moreover, higher permeabilities mostly result in higher solubility coefficients. Lastly, 0% PCL membrane showed always higher permeabilities and diffusion coefficients while PU10 revealed higher solubility coefficients.

Similarly to permeabilities, it is important to note that ANOVA tests were run to all the results presented above and was proved that, for a confidence level of 95%, there was a significant difference between the mean values for diffusion coefficients, as well as for solubility coefficients.

6.3 Surface and Cross-section characterization of Integral Asymmetric Poly(ester urethane urea) membranes by SEM

Following the same procedure adopted in section 6.1, diverse samples of the synthesized membranes varying the PCL content and solvent evaporation time were observed by Scanning Electron Microscopy, to study the influence of said parameters in membrane morphology. Images from both top and bottom surfaces and cross-sections were taken as shown in figures 6.8, 6.9 and 6.10 below.

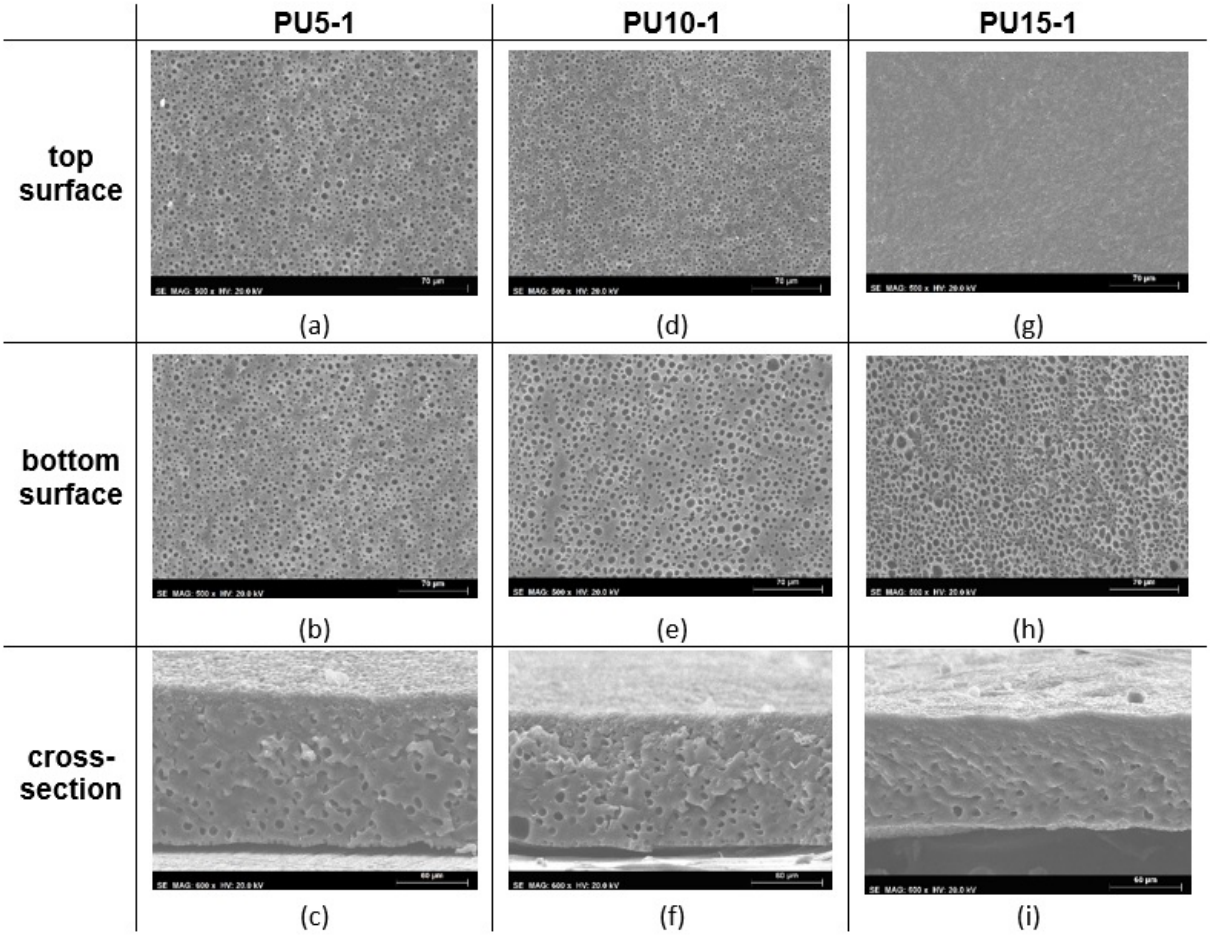

Figure 6.8: Images of the top/bottom surfaces and cross-sections obtained by SEM: (a) top surface, (b) bottom surface and (c) cross-section of membrane PU5-1; (d) top surface, (e) bottom surface and (f) cross-section corresponding to membrane PU10-1; (g) top surface, (h) bottom surface and (i) cross-section of membrane PU15-1.

First, analyzing the images gathered in figure 6.8, it was observed that for the same solvent evaporation times, the amount of pores present on the top surface decreases with the increase in PCL concentration. On the other hand, on the bottom surface, the exact opposite occurred since with the increase in PCL content there was an increase in pore density, with the consequent appearance of pores with a larger diameter. Finally, the decrease in thickness for membranes with a larger contents of said polymer is visible in the cross sections obtained by SEM, reinforcing the accuracy of the measurements performed on every sample and presented in table 6.7 below.

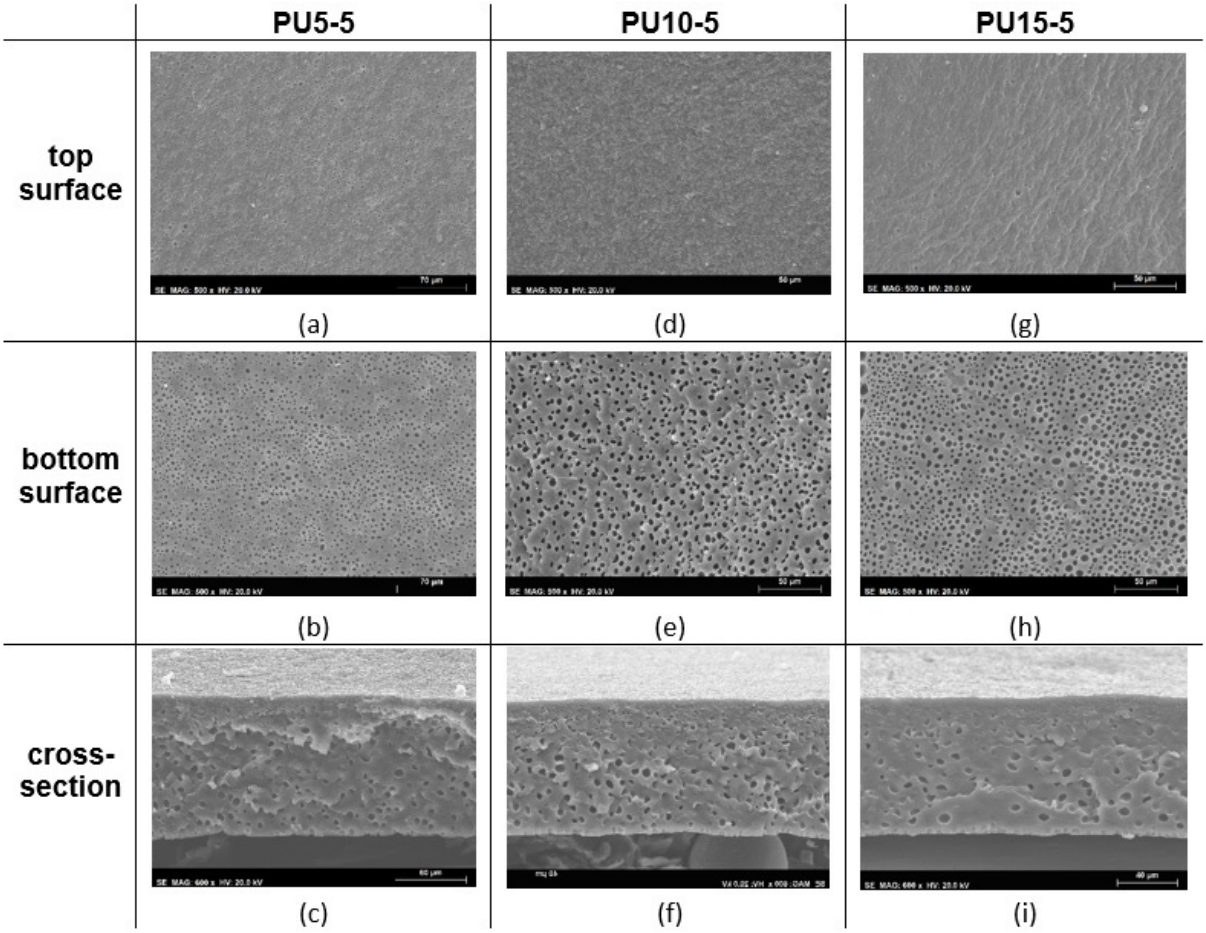

Figure 6.9: Images of the top/bottom surfaces and cross-sections obtained by SEM: (a) top surface, (b) bottom surface and (c) cross-section of membrane PU5-5; (d) top surface, (e) bottom surface and (f) cross-section corresponding to membrane PU10-5; (g) top surface, (h) bottom surface and (i) cross-section of membrane PU15-5.

Next, in figure 6.9 are reported the images referring to the second solvent evaporation time studied. From these images it was possible to conclude that in the present case, an increase in the amount of PCL did not reflect major changes in the characteristics of the top surface of the membrane, only a minor extinction of the residual pores existing in the first composition. In contrast, on the bottom surface, the pore density increases with the concentration of PCL as well as the size of the pores. Lastly, from the observation of the cross sections it was possible to verify that in the core of the membrane, for a concentration of Poly(caprolactone) equal to 10%, the porosity is higher than in the other compositions.

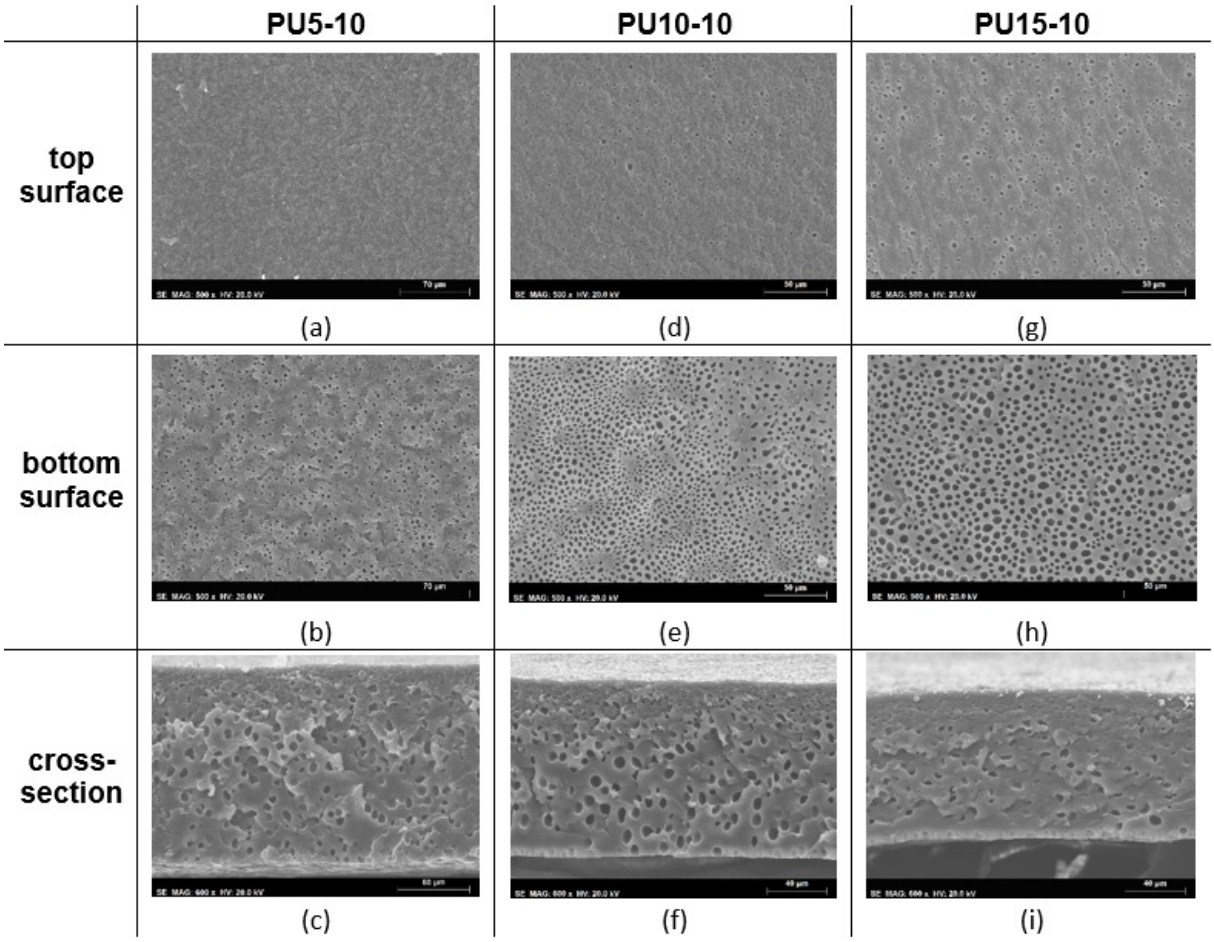

Figure 6.10: Images of the top/bottom surfaces and cross-sections obtained by SEM: (a) top surface, (b) bottom surface and (c) cross-section of membrane PU5-10; (d) top surface, (e) bottom surface and (f) cross-section corresponding to membrane PU10-10; (g) top surface, (h) bottom surface and (i) cross-section of membrane PU15-10.

SEM images obtained for the last solvent evaporation time of 10 minutes are synthesized in figure 6.10. Compared to what was previously stated from the images above, the top surface of the membrane revealed that an increase in PCL content caused a slight increase in porosity. As for the bottom surface, again, an increase in polymer concentration reflects an increase in porosity as well as individual pore size. Similarly to figure 6.9, the observation of the cross sections made it possible to verify that for a PCL amount equal to 10% the membrane's core showed a higher porosity and larger pores than the other compositions. The decrease in membrane thickness is also visible with the increase of PCL.

Comparing now the three figures, and thus also perceiving the effect of the increase of the solvent evaporation time on the morphology of the membranes, a decrease of the pore density on the top surfaces is visible with the increase of the time, except for the membranes with composition equal to 15% PCL. Moreover, the size of the pores does not seem to have any direct relation with the increase of the solvent evaporation time.

However, in general, a lower (almost nonexistent) porosity in the top surface in relation to the bottom surface is noticeable, exhibiting what appears to be a dense thin superficial layer. These dense layers are more easily observed in all membranes containing 15% PCL. Furthermore, the membrane's core does not appear to be completely dense which should facilitate gas permeation.

It is important to note that when the samples were prepared and cut for SEM, regarding its elastomeric and sticky nature, it might not have been achieved a clean cut of the pieces. Moreover, When

ready for testing, porous membranes had a whitish and opaque appearance, were more elastic and easier to operate than nonporous.

Similarly, average total membrane thickness was determined from four different measurements in each sample using a digital caliper. Table 6.7 presents these values as well as the respective standard deviations.

Table 6.7: Average thicknesses and respective standard deviations for integral asymmetric membranes.

Membrane	**Thickness, δ (mm)**
PU5-1	0.118$\pm$0.004
PU10-1	0.117$\pm$0.004
PU15-1	0.102$\pm$0.002
PU5-5	0.107$\pm$0.004
PU10-5	0.109$\pm$0.004
PU15-5	0.103$\pm$0.005
PU5-10	0.121$\pm$0.002
PU10-10	0.121$\pm$0.002
PU15-10	0.110$\pm$0.003

Regarding the thicknesses, due to the difficulty of visualising the dense layer in some of the images, it was considered the total cross-sectional measured values. Furthermore, it is noticeable that membranes with higher contents in PCL were somewhat thinner than the 5 and 10 wt.%. Besides that, the values obtained were in accordance between different samples.

Obtaining different surface and internal morphological characteristics may require an optimisation process of the membrane preparation method, such as the variation of the solvent/solvent and/or polymer/solvent ratios.

6.4 Gas Permeation Experiments - Integral Asymmetric Poly(ester urethane urea) membranes

6.4.1 Different Solvent Evaporation Times

As previously performed on nonporous Poly(ester urethane urea), to evaluate gas permeation of integral asymmetric membranes, several experiments were run applying a constant volume method where the pressure evolution was recorded, using the apparatus described in section 5.5. The tests were performed with multiple feed pressures, as well.

From identical permeation curves to those presented in figure 6.2, plots with fluxes as a function of Transmembrane Pressure were drawn. These plots are organised by membrane type (wt.% PCL and solvent evaporation time) and permeated gas, as shown in figures 6.11, 6.12 and 6.13.

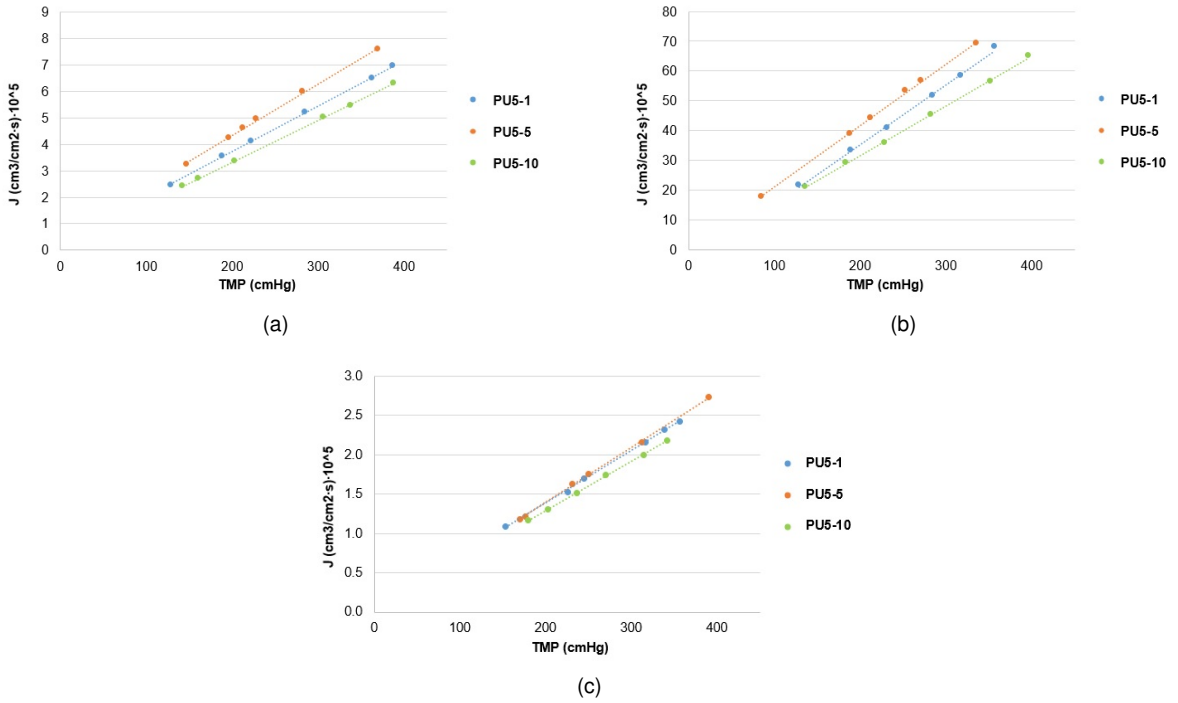

Figure 6.11: Volumetric fluxes as a function of TMP for integral asymmetric PU5 with solvent evaporation times of 1, 5 and 10 minutes: (a) O_2, (b) CO_2 and (c) N_2.

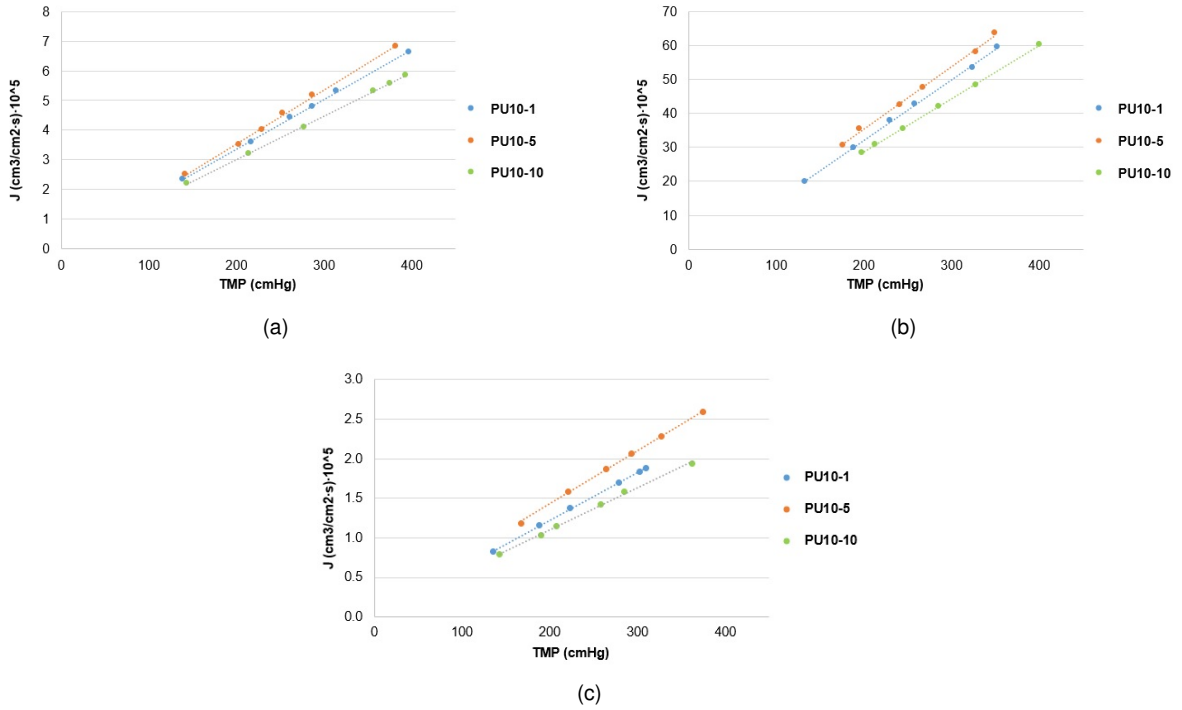

Figure 6.12: Volumetric fluxes as a function of TMP for integral asymmetric PU10 with solvent evaporation times of 1, 5 and 10 minutes: (a) O_2, (b) CO_2 and (c) N_2.

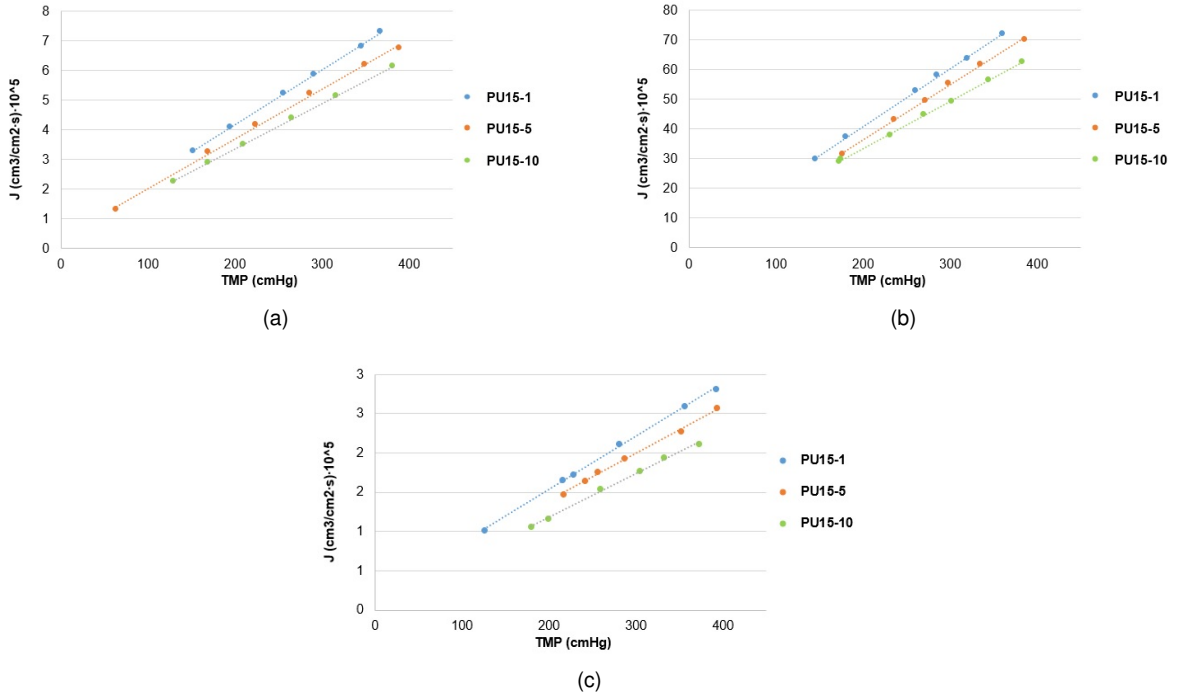

Figure 6.13: Volumetric fluxes as a function of TMP for integral asymmetric PU15 with solvent evaporation times of 1, 5 and 10 minutes: (a) O_2, (b) CO_2 and (c) N_2.

As observed for nonporous membranes, would be expected that the highest fluxes were registered for CO_2, followed by O_2 and then N_2, as it was checked by analyzing the figures above.

Looking now to figures 6.11 and 6.12 by themselves, a clear conclusion to take is the inversion of or-

der for membranes with 1 minute and 5 minutes of solvent evaporation. Keeping in mind the procedure used to prepare integral asymmetric membranes, in principal, longer evaporation times would correspond to thicker dense layers and, consequently, less permeation fluxes. However, this tendency is only revealed in figure 6.13 for 15 wt.% PCL. Again, irregularities in the thickness of the whole membrane taken from the glass and from which the samples were taken can cause differences in the thickness of each sample itself, increasing the disparity of the results.

Once more, knowing the behavior of the fluxes as functions of the TMP for all 9 membranes studied and as a result of the treatment of the slopes through the equation 6.4, it was possible to determine the permeances, $perm$, for each case (table 6.8). It is noteworthy to mention that these results greatly depend on the thickness of the sample used.

Table 6.8: Average permeances determined for integral asymmetric membranes: PU5-1, PU5-5, PU5-10, PU10-1, PU10-5, PU10-10, PU15-1, PU15-5 and PU15-10, prepared with different solvent evaporation times.

	Perm ($cm^3/cm^2\,s\,cmHg$)$\times 10^{-5}$		
Membrane	**O_2**	**CO_2**	**N_2**
PU5-1	0.0180	0.190	0.0066
PU5-5	0.0188	0.200	0.0070
PU5-10	0.0160	0.165	0.0062
PU10-1	0.0162	0.165	0.0060
PU10-5	0.0169	0.179	0.0067
PU10-10	0.0145	0.154	0.0053
PU15-1	0.0187	0.200	0.0068
PU15-5	0.0175	0.184	0.0060
PU15-10	0.0155	0.161	0.0055

In this regard, although some differences were visible between compositions and solvent evaporation times, since the fluxes measured were distinct it was noticeable that the slopes, more specifically the permeances, did not vary so significantly and presented the same order of magnitude.

Membranes synthesized with 5% and 10% PCL and a solvent evaporation time of 5 minutes showed the highest permeances, followed by those with 1 minute and 10 minutes, while 15 wt.% PCL membranes exhibited decreasing values in the order of 1, 5 and 10 minutes.

As previously mentioned, the only values gathered for every sample used on the experiments were the total membrane thicknesses due to the difficulty of visualizing the dense layer in some of the images shown in section 6.3 and being impossible to measure manually. The problem was that as only the dense layer of these membranes, thus only a fraction of the prior determined values, offers resistance to the gas permeation, computing the permeabilities was unachievable.

6.4.2 Different PCL contents

The set of data gathered during the experiments made it possible to evaluate if there was any type of correlation between the amount of PCL polymer in the membranes and the permeability properties, as well.

Figures 6.14, 6.15 and 6.16 equally represent plots of the volumetric fluxes as a function of Transmembrane Pressure (TMP) for every composition studied (5%, 10% and 15% PCL), maintaining the solvent evaporation time constant.

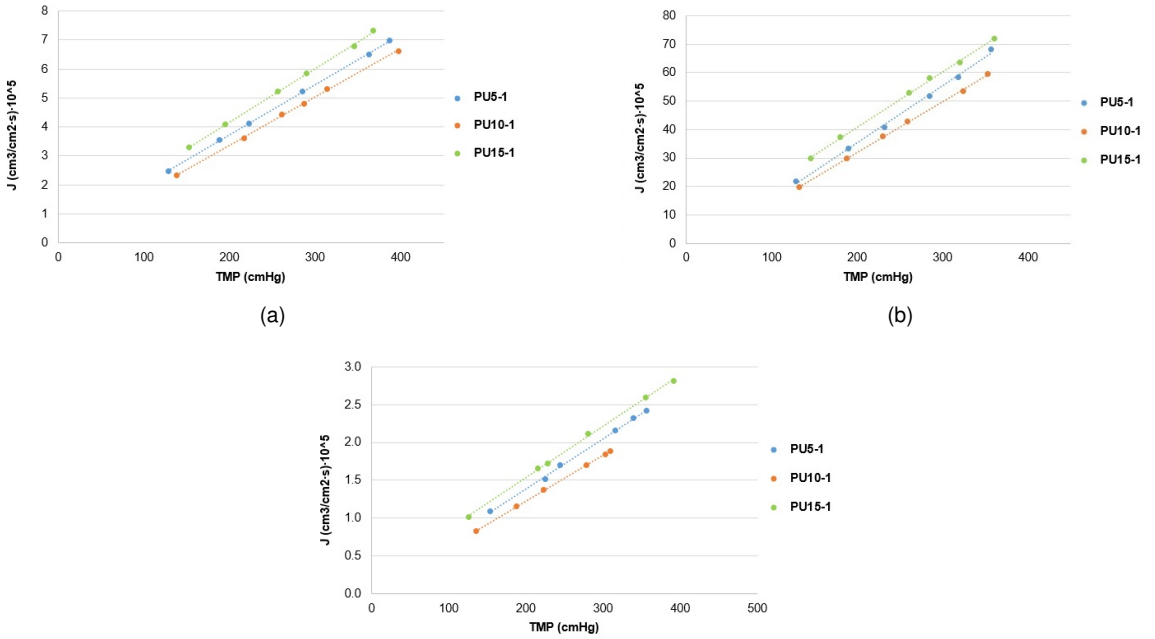

Figure 6.14: Volumetric fluxes as a function of TMP for integral asymmetric PU5, PU10 and PU15 with solvent evaporation time of 1 minute: (a) O_2, (b) CO_2 and (c) N_2.

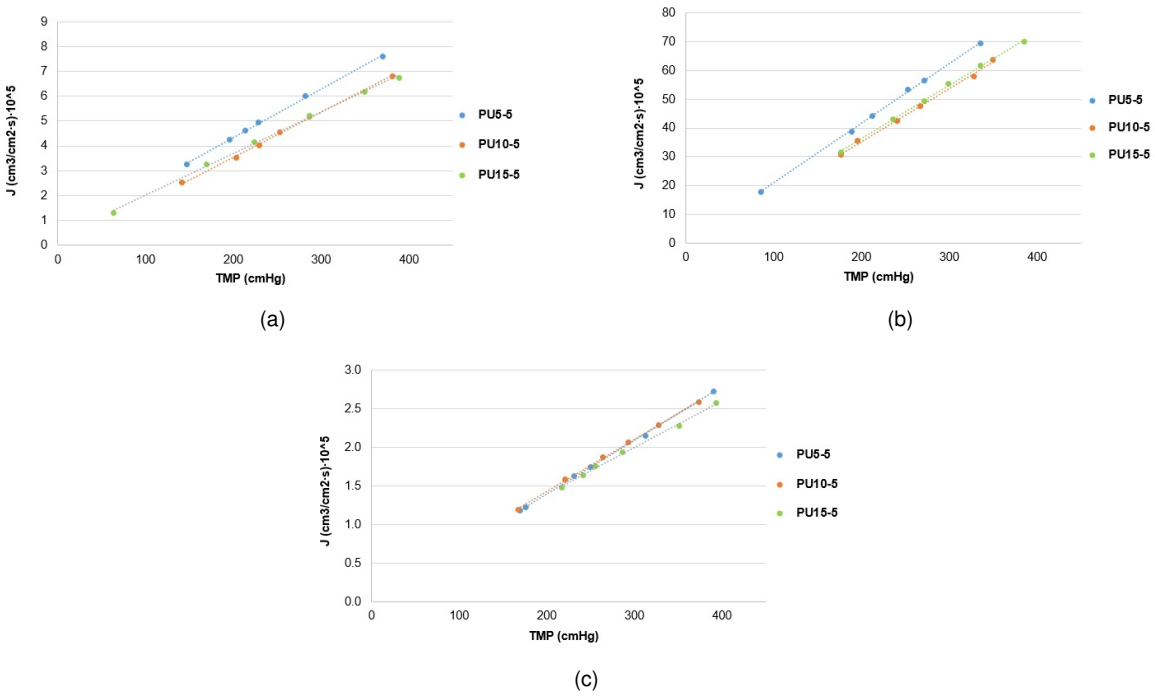

Figure 6.15: Volumetric fluxes as a function of TMP for integral asymmetric PU5, PU10 and PU15 with solvent evaporation time of 5 minutes: (a) O_2, (b) CO_2 and (c) N_2.

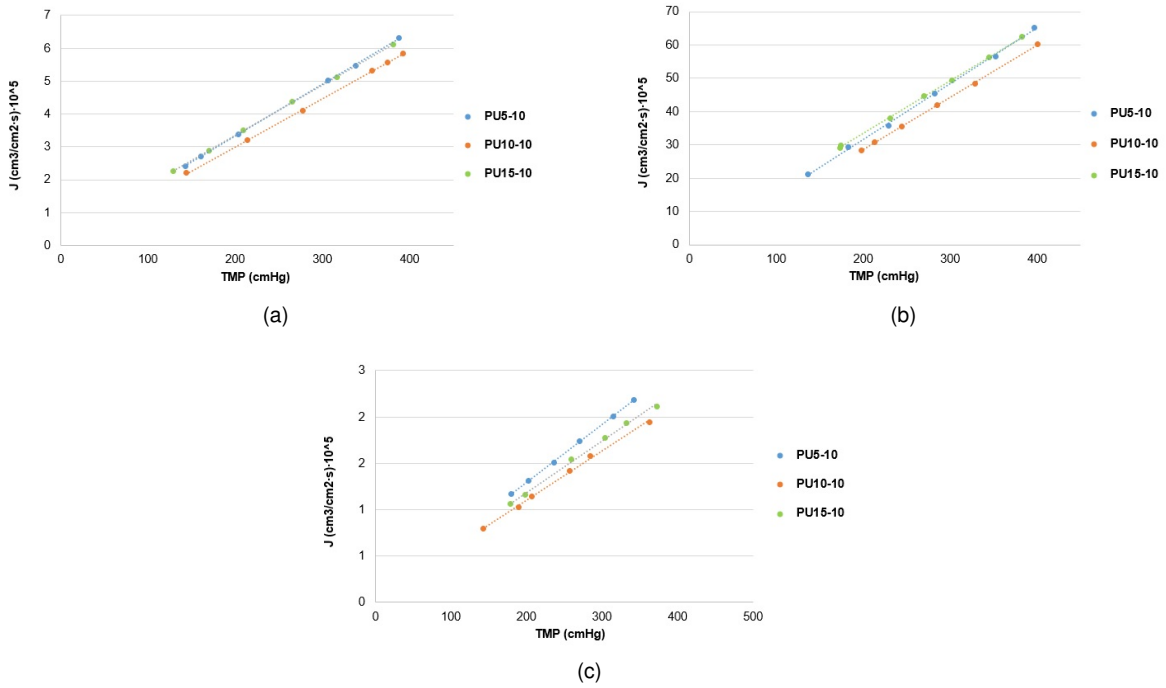

Figure 6.16: Volumetric fluxes as a function of TMP for integral asymmetric PU5, PU10 and PU15 with solvent evaporation time of 10 minutes: (a) O_2, (b) CO_2 and (c) N_2.

Analyzing the three figures shown above, the good performance of the membranes synthesized with the lowest and highest amount of PCL was evidenced. On the reverse, in general, the intermediate composition registered the lowest volumetric fluxes. It is also important to point out the membrane inversion for evaporation times of 1 and 5 minutes, in other words, while for the first evaporation time the membrane that revealed the highest flux was the one with the highest amount of the mentioned polymer (15 %wt), for the second was the one with the lowest composition (5 %wt) that was the one exceeding the remaining ones. Finally, for 10 minutes of solvent evaporation time the results are in accordance between the different membranes.

Table 6.9: Average permeances determined for integral asymmetric membranes: PU5-1, PU5-5, PU5-10, PU10-1, PU10-5, PU10-10, PU15-1, PU15-5 and PU15-10, prepared with different PCL contents.

	Perm ($cm^3/cm^2\,s\,cmHg)\times10^{-5}$		
Membrane	O_2	CO_2	N_2
PU5-1	0.0180	0.190	0.0066
PU10-1	0.0162	0.165	0.0060
PU15-1	0.0187	0.200	0.0068
PU5-5	0.0188	0.200	0.0070
PU10-5	0.0169	0.179	0.0067
PU15-5	0.0175	0.184	0.0060
PU5-10	0.0160	0.165	0.0062
PU10-10	0.0145	0.154	0.0053
PU15-10	0.0155	0.161	0.0055

Observing all results synthesized in table 6.9, the lower values were always obtained for 10% PCL membrane, excepting for N_2 with 5 minutes of solvent evaporation. Respecting the other two compositions, when prepared with 5 and 10 minutes a decrease in permeance was verified from the 5 to 15% PCL for O_2, CO_2 and N_2. For membranes with 1 minute of solvent evaporation, the opposite was ob-

served instead. With this being said, it was not possible to find a direct correlation between the amount of PCL and the permeances with the same trend observed for the fluxes being followed as seen before in section 6.4.1.

6.4.3 Comparing Nonporous with Integral Asymmetric Poly(ester urethane urea) membranes

With the goal of comparing the gas permeation characteristics of both nonporous and integral asymmetric Poly(ester urethane urea) (PEUU) membranes and investigate if there was any benefits on using the latter on actual blood oxygenators, once it was not possible to compare permeabilities or diffusion and solubility coefficients, the volumetric fluxes obtained during the experiments were gathered in the figures displayed below.

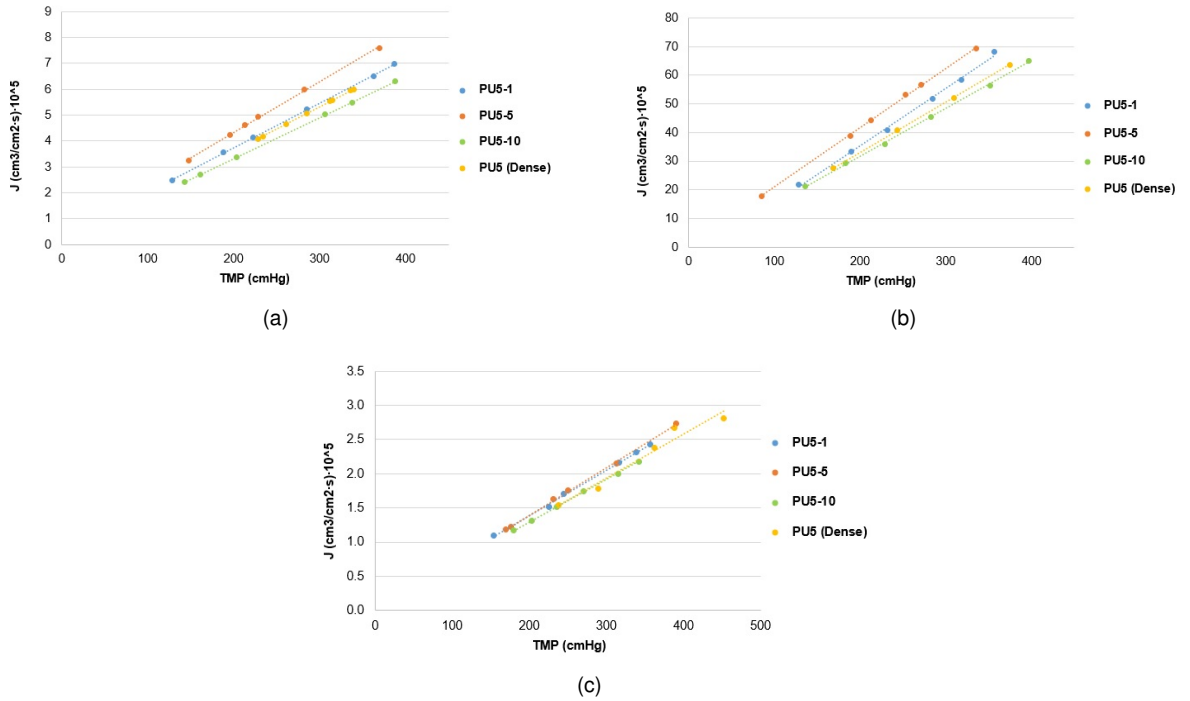

Figure 6.17: Volumetric fluxes as a function of TMP for dense PU5 and integral asymmetric PU5 with solvent evaporation times of 1, 5 and 10 minutes: (a) O_2, (b) CO_2 and (c) N_2.

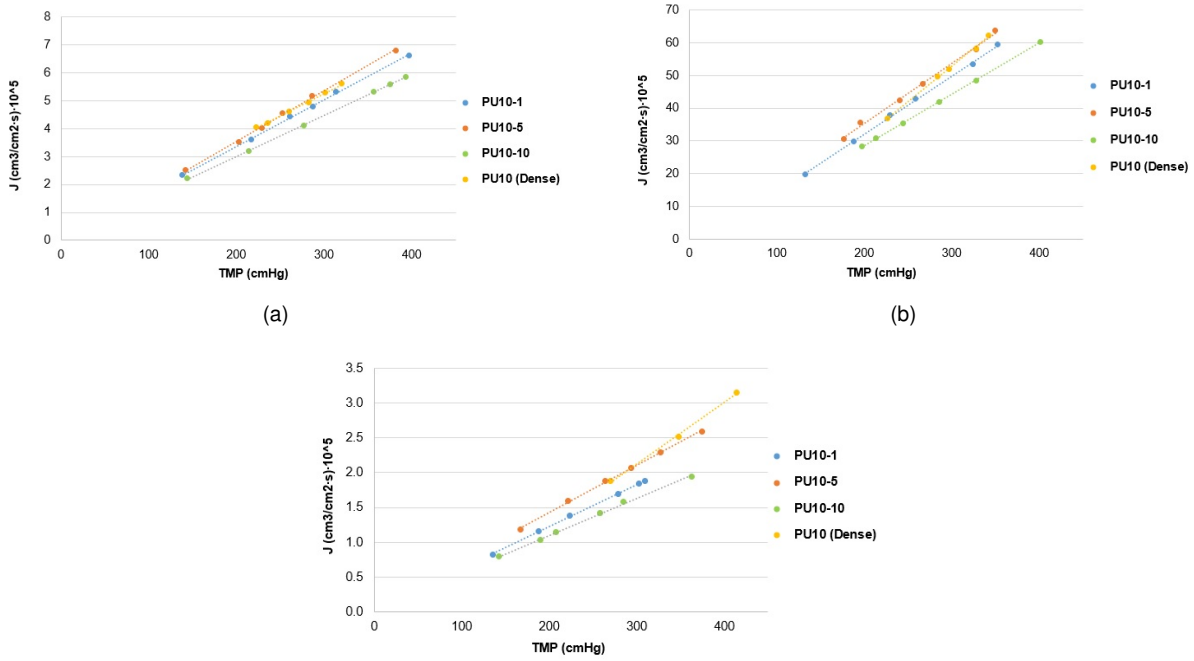

Figure 6.18: Volumetric fluxes as a function of TMP for dense PU10 and integral asymmetric PU10 with solvent evaporation times of 1, 5 and 10 minutes: (a) O_2, (b) CO_2 and (c) N_2.

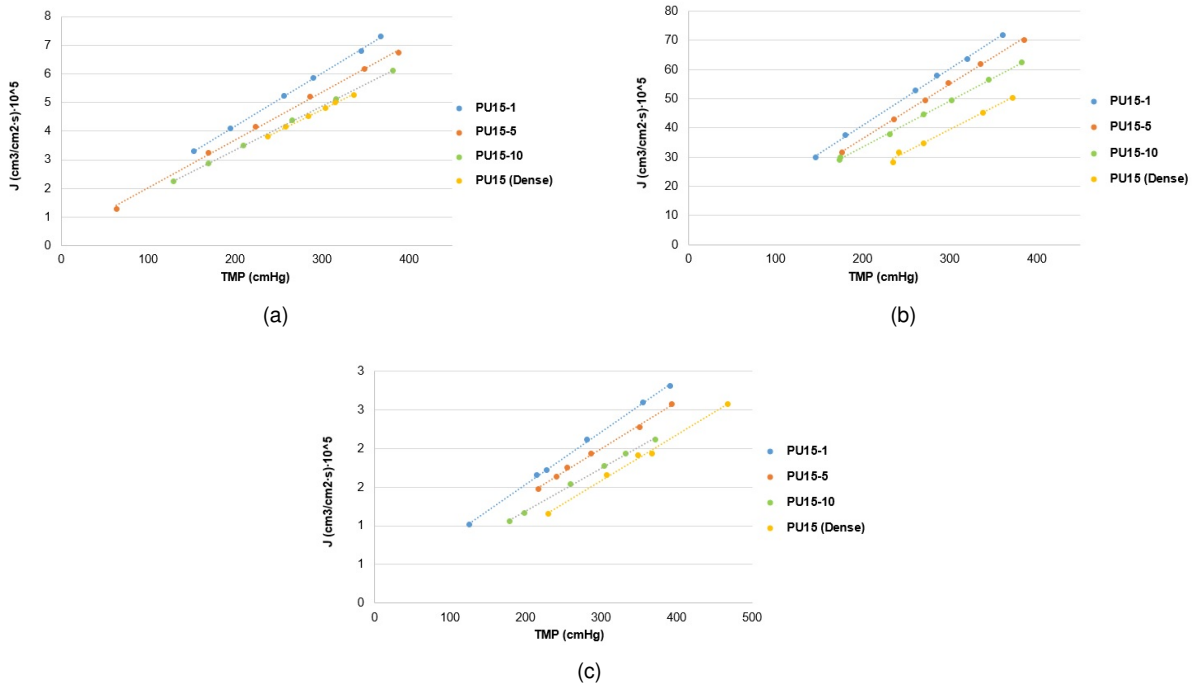

Figure 6.19: Volumetric fluxes as a function of TMP for dense PU15 and integral asymmetric PU15 with solvent evaporation times of 1, 5 and 10 minutes: (a) O_2, (b) CO_2 and (c) N_2.

Analyzing the behavior of the volumetric fluxes for every gas and PCL content, it can be seen that not every dense membrane appears below all asymmetric, meaning that some compositions do not represent any improvement despite their asymmetric character. Moreover, this results support what was stated when the thicknesses of dense layers were estimated and showed an improvement in gas

permeation for PU5-1, PU5-5, PU15-1, PU15-5 and PU15-10, as shown below in this section.

From figures 6.17 and 6.18, a quick conclusion to withdrawn is asymmetric membranes with 5% and 10% PCL with 5 minutes of solvent evaporation time appear to be the best composition and have the optimal mode of preparation, along the fact that 5 wt.% was the most promising for medical devices requiring a short-term contact with blood and showed strong assets on the design of membranes with enhanced hemocompatibility, mainly with regard to platelet adhesion, as revealed in previous studies [13]. In addition, it is also known that states of fully spread platelet activation is inhibited for PCL contents of 5% [16].

Observing now figure 6.19, unlike other compositions, the membrane that showed the best performance was the one with only 1 minute of solvent evaporation time. In addition, extreme states of platelet activation, spread and fully spread, are inhibited in membranes with 15 wt.% PCL [16].

Furthermore, to complete the comparison between the two types of membranes, assuming that the morphology of the dense layer of an asymmetric membrane is equal to a totally dense, which means that the characteristics remain the same, the thicknesses of the dense layers could be estimated using the permeabilities of nonporous Poly(ester urethane urea) (table 6.2) by applying the permeance values obtained for the asymmetric, as expression 6.6 presents:

$$\delta = \frac{P}{perm \times 10^{10}} \tag{6.6}$$

Thereby, estimated values for dense layer's thickness are reported in table 6.10.

Table 6.10: Average estimated thicknesses and respective standard deviations for integral asymmetric membranes.

Membrane	**Estimated Thickness, δ (mm)**
PU5-1	0.109±0.004
PU5-5	0.104±0.005
PU5-10	0.122±0.003
PU10-1	0.132±0.021
PU10-5	0.122±0.016
PU10-10	0.145±0.024
PU15-1	0.089±0.005
PU15-5	0.097±0.008
PU15-10	0.109±0.007

The determination of this estimated values enabled the comparison with the ones in table 6.7 - total membrane thickness. This comparison is schematized in figure 6.20.

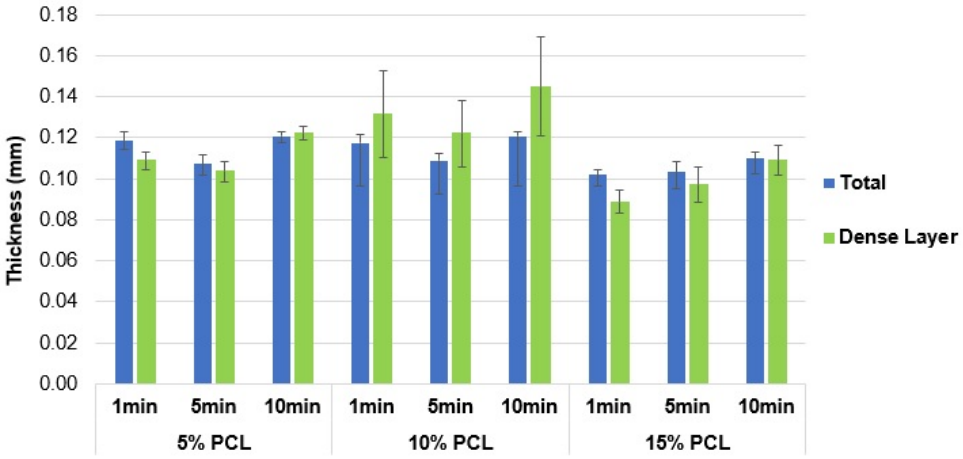

Figure 6.20: Comparison of total membrane thicknesses measured and estimated thickness values for integral asymmetric membranes.

Despite the results obtained for 10% PCL membranes where the estimated thicknesses were all higher than total membrane measured manually, which is not physically acceptable, for the remaining 2 compositions it was possible to observe a decrease of the variable under study (δ). Therefore, can be affirmed that, in this conditions, preparing an integral asymmetric instead of a totally dense membrane allowed a reduction of 8%, 3%, 13%, 6% and 1% of the dense layer for PU5-1, PU5-5, PU15-1, PU15-5 and PU15-10, respectively.

In fact, the permeance values obtained for the nonporous symmetric membranes present the same order of magnitude as the asymmetric membranes. These results may be due to the fact that the so-called asymmetrical membranes are not entirely asymmetrical. This means that the pores observed on the bottom surface may not be interconnected so the gas molecules will have to diffuse from pore to pore through the membranes' core, acting like a dense membrane. Once more, the problem may lie in the preparation of said membranes, more specifically, in the type of prepolymers used, the proportions between polymers and solvents or solvents among themselves and the solvent evaporation times, which maybe can be lowered.

Chapter 7

Conclusion

Experimental tests were performed in a setup designed and optimized to allow high degrees of reproducibility and low uncertainty. This system aims to obtain more precise gas permeation measurements of membranes at a constant temperature and volume, by varying the feed pressure and monitoring the pressure difference evolution over time. Measurements were taken for three distinct gases, namely nitrogen, oxygen and carbon dioxide with inlet pressures between 1 bar and 5 bar and using volumes of 13.5 cm^3 for the first two gases and 193.3 cm^3 for the last, due to the sensibility of the equipment.

Nonporous Poly(ester urethane urea) (PEUU) membranes were prepared using the solvent evaporation method with a solvent ratio (DMF/DEE) of 3/1 wt.% and a polymer/solvent ratio of 65/35 wt.%. Regarding the polymer compositions used, four different amounts of Poly(caprolactone) (PCL) were studied being 0, 5, 10 and 15 wt.% corresponding to a 100, 95, 90 and 85 wt.% content of Polyurethane (PU) (PU0, PU5, PU10 and PU15, respectively). Scanning Electron Microscopy revealed completely dense surfaces (top and bottom), as well as the cross sections. When ready to use, said membranes were transparent, very sticky and slightly elastic, with average thicknesses of 0.112±0.006 mm, 0.115±0.004 mm, 0.107±0.004 mm and 0.112±0.001 mm, respectively.

Regarding the properties determined for nonporous PEUU, permeability, diffusion and solubility coefficients were calculated. The O_2 permeabilities assumed values equal to 22.9±0.4 Barrer, 20.1±0.3 Barrer, 18.2±0.4 Barrer and 16.5±0.5 Barrer while diffusion coefficients were $(2.14 \pm 0.44) \times 10^{-6} cm^2/s$, $(1.91 \pm 0.16) \times 10^{-6} cm^2/s$, $(1.59 \pm 0.20) \times 10^{-6} cm^2/s$ and $(1.74 \pm 0.12) \times 10^{-6} cm^2/s$ and solubility coefficients $(11.13 \pm 1.68) \times 10^{-4} cm^3/cm^3 cmHg$, $(10.64 \pm 0.93) \times 10^{-4} cm^3/cm^3 cmHg$, $(11.86 \pm 2.14) \times 10^{-4} cm^3/cm^3 cmHg$ and $(9.62 \pm 1.21) \times 10^{-4} cm^3/cm^3 cmHg$, for PU0, PU5, PU10 and PU15, respectively.

Concerning CO_2 and the variables determined, values equal to 230±0 Barrer, 198.3±1.3 Barrer, 218.0±36.1 Barrer and 168.1±0.5 Barrer for permeabilities while diffusion coefficients were $(1.66 \pm 0.15) \times 10^{-6} cm^2/s$, $(1.63 \pm 0.15) \times 10^{-6} cm^2/s$, $(1.36 \pm 0.08) \times 10^{-6} cm^2/s$ and $(1.42 \pm 0.08) \times 10^{-6} cm^2/s$ and solubility coefficients $(140.01 \pm 11.80) \times 10^{-4} cm^3/cm^3 cmHg$, $(123.25 \pm 12.92) \times 10^{-4} cm^3/cm^3 cmHg$, $(160.03 \pm 8.50) \times 10^{-4} cm^3/cm^3 cmHg$ and $(119.22 \pm 7.38) \times 10^{-4} cm^3/cm^3 cmHg$, for PU0, PU5, PU10 and PU15, respectively.

Finally, the results for N_2 were 9.9 Barrer, 7.4 Barrer, 10.1 Barrer and 6.7 Barrer for permeabilities while diffusion coefficients were $(1.40 \pm 0.05) \times 10^{-6} cm^2/s$, $(1.22 \pm 0.11) \times 10^{-6} cm^2/s$, $(1.22 \pm 0.14) \times 10^{-6} cm^2/s$ and $(1.00 \pm 0.02) \times 10^{-6} cm^2/s$ and solubility coefficients $(7.07 \pm 0.24) \times 10^{-4} cm^3/cm^3 cmHg$, $(6.14 \pm 0.60) \times 10^{-4} cm^3/cm^3 cmHg$, $(8.40 \pm 1.00) \times 10^{-4} cm^3/cm^3 cmHg$ and $(6.74 \pm 0.16) \times 10^{-4} cm^3/cm^3$ cmHg in the same order of membranes.

Overall, it was possible to conclude that the highest fluxes were registered for CO_2, followed by O_2 and N_2, and higher permeabilities mostly result in higher solubility coefficients. Moreover, apart from the successive decrease in permeabilities for O_2 with the increase in PCL content, it was not possible to

find a trend relating permeabilities, diffusion and solubility coefficients with the increase of said polymer, in the conditions described. Also, knowing the capacity of performance of the ideal oxygenator and considering a constant feed pressure of 2 bar, the membrane surface areas estimated varied between 13.5-17.5 m^2 for O_2 and 1.2-1.7 m^2 for CO_2, which means the first gas is the limiting factor in membranes development when it comes to active surface areas. On the other hand, better hemocompatibility of the present membranes can make up the verified deficit on the O_2 side.

Further on, integral asymmetric PEUU were synthesized applying a modified phase inversion method, maintaining DMF/DEE proportions as well as the polymer/solvent ratio used for nonporous membranes, except the 0% PCL one. The times studied in the solvent evaporation phase, before consequent immersion in water, were 1, 5 and 10 minutes and measured thicknesses varied between 0.102 mm and 0.121 mm.

Scanning Electron Microscopy showed that for the same solvent evaporation time, the amount of pores presented on the top surfaces decreases with the increase in PCL concentration, except for the 10 minutes evaporation time. Regarding the bottom surfaces, the exact opposite occurred since with the increase in PCL content there was an increase in pore density, as well as in pore diameter for evaporation times of 5 and 10 minutes. Finally, cross sections enabled the perception that for a polymer amount equal to 10% means higher porosity and larger pores when compared to other compositions. SEM also revealed a decrease in pore density on the top surfaces with the increase of evaporation time, except for membranes with compositions equal to 15% PCL. In all membranes was possible to observe a thin superficial layer that appears to be totally or almost totally dense. Contrary to what has been observed for symmetrical membranes, when ready for testing, porous membranes had a whitish and opaque appearance, were more elastic and easier to operate.

After comparing the effects of the different evaporation times applied and the 3 compositions studied, it was concluded that apart from the fact that the largest fluxes continue to be observed for carbon dioxide, the permeance values, did not present great disparities with the variation of these variables. Also, no direct relationship was found between solvent evaporation time or wt.% of PCL used with permeances.

Estimates made on the thickness of the dense layer revealed that the synthesis of asymmetrical membranes allowed a reduction of 8%, 3%, 13%, 6% and 1% for PU5-1, PU5-5, PU15-1, PU15-5 and PU15-10, in contrast to fully dense membranes. This result supported the improvement verified in gas permeation.

However, besides reviewing the preparation steps, the possible problems of reproducibility in the preparation of asymmetrical membranes, as well as the synthesis of thinner membranes with satisfactory resistance, could be solved by introducing the manufacture of supported membranes.

Finally, from the comparison of both types of membranes, including all three different compositions and the diverse evaporation times, it was possible to realize that the best compositions and, consequently, preparation methods were 5% PCL with 5 minutes of solvent evaporation time and 15% PCL with 1 minute of solvent evaporation time.

Chapter 8

Perspectives for Future work

Next step would consist in testing all the same membranes reported in the present work in a gas-liquid system to make sure the behaviour observed is consistent, since in a real ECMO the exchange is carried out through a membrane from blood to gas and vice versa.

Furthermore, having selected the membranes with the best performance, it would be of great interest to introduce microfibers on the surface of the active layer, for example, through an electrospining technique, in order to promote the mixing and disruption of the diffusive boundary layer and improve mass transfer.

Gas permeation of modified membranes must be tested in both existing gas/membrane/gas setup, as well as in the gas/membrane/liquid.

Plus, manufacturing supported membranes would be important to eliminate possible problems of reproducibility as well as improving the resistance of thinner membranes. Characterization and gas permeation tests in gas-gas and gas-liquid systems are necessary.

Bibliography

[1] "Membranes for the Life Sciences," in *Membrane Technology* (K.-V. Peinemann and S. Pereira Nunes, eds.), vol. 1, Wiley-VCH, 2007.

[2] N. C. Nanda, N. Trehan, B. Airan, S. A. Conrad, and Y. Mehta, *Manual of Extracorporeal Membrane Oxygenation (ECMO) in the ICU*. 2014.

[3] H. Iwahashi, K. Yuri, and Y. Nosé, "Development of the oxygenator: Past, present, and future," *Journal of Artificial Organs*, vol. 7, no. 3, pp. 111–120, 2004.

[4] D. F. Stamatialis, B. J. Papenburg, M. Giron, S. N. M. Bettahalli, S. Schmitmeier, and M. Wessling, "Medical applications of membranes : Drug delivery , artificial organs and tissue engineering," vol. 308, pp. 1–34, 2008.

[5] S. Sun, Y. Yue, X. Huang, and D. Meng, "Protein adsorption on blood-contact membranes," *Journal of Membrane Science*, vol. 222, no. 1-2, pp. 3–18, 2003.

[6] M. D. Lelah, J. A. Pierce, L. K. Lambrecht, and S. L. Cooper, "Polyether-urethane ionomers: surface property/ex vivo blood compatibility relationships," *Journal of Colloid And Interface Science*, vol. 104, no. 2, pp. 422–439, 1985.

[7] H. J. Griesser, "Degradation of polyurethanes in biomedical applications-A review," *Polymer Degradation and Stability*, vol. 33, no. 3, pp. 329–354, 1991.

[8] R. Deppisch, M. Storr, R. Buck, and H. Göhl, "Blood material interactions at the surfaces of membranes in medical applications," *Separation and Purification Technology*, vol. 14, no. 1-3, pp. 241–254, 1998.

[9] M. Faria and M. N. de Pinho, "Phase segregation and gas permeation properties of poly(urethane urea) bi-soft segment membranes," *European Polymer Journal*, vol. 82, pp. 260–276, 2016.

[10] M. Ferreira Marques, P. M. Gordo, C. Lopes Gil, A. P. de Lima, D. Placco Queiroz, M. Norberta de Pinho, Z. Kajcsos, and G. Duplâtre, "Gas Permeability and Temperature-Dependent Free-Volume Studies in Polyurethane Membranes by Positron Lifetime and Doppler Spectroscopies," *Materials Science Forum*, vol. 445-446, pp. 289–291, 2009.

[11] M. I. Pinto, D. P. Queiroz, M. H. Gil, A. J. Guiomar, and M. Norberta de Pinho, "Polyurethane-Polyurea Membranes for Blood Oxygenation," *Materials Science Forum*, vol. 514-516, pp. 863–867, 2006.

[12] D. P. Queiroz and M. N. De Pinho, "Structural characteristics and gas permeation properties of polydimethylsiloxane/poly(propylene oxide) urethane/urea bi-soft segment membranes," *Polymer*, vol. 46, no. 7, pp. 2346–2353, 2005.

[13] M. C. Besteiro, A. J. Guiomar, C. A. Gonçalves, V. A. Bairos, M. N. De Pinho, and M. H. Gil, "Characterization and in vitro hemocompatibility of bi-soft segment, polycaprolactone-based poly(ester urethane urea) membranes," *Journal of Biomedical Materials Research - Part A*, vol. 93, no. 3, pp. 954–964, 2010.

[14] M. Faria, V. Geraldes, and M. N. De Pinho, "Surface characterization of asymmetric Bi-soft segment poly(ester urethane urea) membranes for blood-oxygenation medical devices," *International Journal of Biomaterials*, vol. 2012, 2012.

[15] S. Matteucci, Y. Yampolskii, B. D. Freeman, and I. Pinnau, *Transport of Gases and Vapors in Glassy and Rubbery Polymers*. 2006.

[16] M. Faria, P. Brogueira, and M. N. de Pinho, "Sub-micron tailoring of bi-soft segment asymmetric polyurethane membrane surfaces with enhanced hemocompatibility properties," *Colloids and Surfaces B: Biointerfaces*, vol. 86, no. 1, pp. 21–27, 2011.

[17] M. Faria, M. Rajagopalan, and M. N. De Pinho, "Tailoring bi-soft segment poly (ester urethane urea) integral asymmetric membranes for CO2 and O2 permeation," *Journal of Membrane Science*, vol. 387-388, no. 1, pp. 66–75, 2012.

[18] M. Brito, "Introduction," in *Basic Principles of Membrane Technology*, pp. 1–18, Springer Netherlands, 2 ed., 2003.

[19] G. S. Park, "Transport Principles—Solution, Diffusion and Permeation in Polymer Membranes," *Synthetic Membranes: Science, Engineering and Applications*, pp. 57–107, 2012.

[20] A. F. Ismail, K. C. Khulbe, and T. Matsuura, *Gas Separation Membranes: Polymeric and Inorganic*. Springer International Publishing, 2015.

[21] R. M. Barrer and E. K. Rideal, "Permeation, diffusion and solution of gases in organic polymers," no. 628, pp. 628–643, 1939.

[22] S. W. Rutherford and D. D. Do, "Review of time lag permeation technique as a method for characterisation of porous media and membranes," *Adsorption*, vol. 3, no. 4, pp. 283–312, 1997.

[23] C. Stropnik; L. Germic; B. Zerjal, "Morphology variety and formation mechanisms of polymeric membranes prepared by wet phase inversion," *Journal of Applied Polymer Science*, vol. 61, no. 10, pp. 1821–1830, 1996.

[24] S. A. Altinkaya, "Modeling of asymmetric membrane formation by a combination of dry/wet phase inversion processes," *Desalination*, vol. 199, no. 1-3, pp. 459–460, 2006.

[25] T. M. Eusébio, "Polyurethane urea membranes for membrane blood oxygenators : synthesis and gas permeation properties," *Instituto Superior Técnico MSc Thesis*, November 2017.

[26] G. Pon, "Gas permeation in bi-soft segment poly (ester urethane urea) membranes for Membrane Blood Oxygenators," *Instituto Superior Técnico MSc Thesis*, November 2018.

[27] F. Wiese, "Membranes for Artificial Lung and Gas Exchange Applications," in *Biomedical Membranes and (Bio)Artificial Organs* (D. Stamatialis, ed.), vol. 2, ch. 4, pp. 83–104, 2018.

[28] D. N. Gray, "Polymeric Membranes for Artificial Lungs.," in *Polymeric Materials and Artificial Organs* (C. G. Gebelein, ed.), ch. 9, pp. 151–162, 1984.

[29] R. W. Baker and B. T. Low, “Gas separation membrane materials: A perspective,” *Macromolecules*, vol. 47, no. 20, pp. 6999–7013, 2014.

[30] R. Perry, D. Green, and J. Maloney, *Chemical Engineer Handbook*. McGraw-Hill, 7 ed., 1997.

[31] M. Mulder, *Basic Principles of Membrane Technology*. Springer Netherlands, 2 ed., 1997.

Appendix A

Time Lag

The gas permeation tests performed on the membranes under study allowed the determination of the intersection of the steady-state asymptote with the x-axis, from the graphic representations of the pressure evolution as a function of time. This same intersection, as explained in section 6.2.2, is called time lag. Table A.1 shows the average values obtained for each membrane, as well as the corresponding permeated gas.

Table A.1: Time lag values obtained from gas permeation curves.

	Time (s)		
Membrane	N_2	O_2	CO_2
PU0	17.28	10.14	11.42
PU5	17.82	11.43	14.02
PU10	18.32	10.13	13.54
PU15	21.12	11.55	14.86

Subsequently, the results reported above contributed to the calculation of the diffusion coefficients, presented in section 6.2.2.